Cell-Based Phenotypic Drug Screening Identifies Luteolin as Candidate Therapeutic for Nephropathic Cystinosis

Ester De Leo,[1] Mohamed A. Elmonem ⬚,[2,3] Sante Princiero Berlingerio,[3] Marine Berquez,[4] Beatrice Paola Festa,[4] Roberto Raso,[1] Francesco Bellomo,[1] Tobias Starborg,[5] Manoe Jacoba Janssen,[6] Zeinab Abbaszadeh,[7] Sara Cairoli,[8] Bianca Maria Goffredo,[8] Rosalinde Masereeuw,[6] Olivier Devuyst,[4] Martin Lowe,[9] Elena Levtchenko,[3] Alessandro Luciani,[4] Francesco Emma,[1,10] and Laura Rita Rega[1]

Due to the number of contributing authors, the affiliations are listed at the end of this article.

ABSTRACT

Background Mutations in the gene that encodes the lysosomal cystine transporter cystinosin cause the lysosomal storage disease cystinosis. Defective cystine transport leads to intralysosomal accumulation and crystallization of cystine. The most severe phenotype, nephropathic cystinosis, manifests during the first months of life, as renal Fanconi syndrome. The cystine-depleting agent cysteamine significantly delays symptoms, but it cannot prevent progression to ESKD and does not treat Fanconi syndrome. This suggests the involvement of pathways in nephropathic cystinosis that are unrelated to lysosomal cystine accumulation. Recent data indicate that one such potential pathway, lysosome-mediated degradation of autophagy cargoes, is compromised in cystinosis.

Methods To identify drugs that reduce levels of the autophagy-related protein p62/SQSTM1 in cystinotic proximal tubular epithelial cells, we performed a high-throughput screening on the basis of an in-cell ELISA assay. We then tested a promising candidate in cells derived from patients with, and mouse models of, cystinosis, and in preclinical studies in cystinotic zebrafish.

Results Of 46 compounds identified as reducing p62/SQSTM1 levels in cystinotic cells, we selected luteolin on the basis of its efficacy, safety profile, and similarity to genistein, which we previously showed to ameliorate other lysosomal abnormalities of cystinotic cells. Our data show that luteolin improves the autophagy–lysosome degradative pathway, is a powerful antioxidant, and has antiapoptotic properties. Moreover, luteolin stimulates endocytosis and improves the expression of the endocytic receptor megalin.

Conclusions Our data show that luteolin improves defective pathways of cystinosis and has a good safety profile, and thus has potential as a treatment for nephropathic cystinosis and other renal lysosomal storage diseases.

Nephropathic cystinosis (Online Mendelian Inheritance in Man [OMIM] 219800) is an autosomal recessive lysosomal storage disease, caused by severe mutations in the *CTNS* gene, which encodes cystinosin, a ubiquitously expressed lysosomal cystine symporter.[1,2] Defective lysosomal transport of cystine leads to intracellular accumulation and crystallization in all organs.[3] Notably, kidneys, and in particular proximal tubular epithelial cells (PTCs), are affected at early stages of the disease, leading to early-onset Fanconi

syndrome and inappropriate urinary losses of water, amino acids, phosphate, bicarbonate, glucose, and low-molecular-weight proteins. Chronic renal failure develops progressively, and most patients reach ESKD at around 10 years of age if not treated with cysteamine. With time, cystine accumulation in other organs causes extrarenal complications, such as hypothyroidism, diabetes mellitus, and myopathy, among others.[4]

Cysteamine is a cystine-depleting agent allowing clearance of cystine from lysosomes, and is currently the only specific treatment for cystinosis. If started early, it significantly delays progression of renal failure, and prevents or delays other complications of the disease.[3] However, cysteamine does not cure cystinosis and does not stop the onset of renal Fanconi syndrome. Moreover, patient compliance is often limited by side effects.[5] Hence, efforts have been made to develop new therapies. A first approach has been to develop modified cysteamine molecules or to identify other cystine-depleting agents with a better therapeutic profile.[6] Hematopoietic stem cell transplantation has recently emerged as a potential therapy, with promising results in mice.[7] Alternatively, new treatments could target pathways that are not responsive to cysteamine. In particular, mechanisms leading to PTC dysfunction are probably not solely related to cystine accumulation because renal Fanconi syndrome is not improved by cysteamine. In this respect, recent studies have identified several defects, including enhanced apoptosis,[8–11] mitochondrial dysfunction,[12,13] oxidative stress,[14–17] aberrant autophagy,[18–20] endo-lysosomal dysfunction,[21,22] and decreased expression of megalin and cubilin.[21,23] Among these, altered autophagy likely plays a pivotal role. Accumulation of the autophagy substrate p62/SQSTM1 has been described in human PTCs and in kidney biopsy specimens, suggesting impaired autophagic flux.[18] Recently, it has been shown that lysosomal dysfunction in primary PTCs obtained from $Ctns^{-/-}$ mice contributes to defective autophagy-mediated clearance of damaged mitochondria.[20] In this hypothesis, defective autophagy, which is unrelated to cystine accumulation,[19] would represent an important target to identify new treatments.

Generally, big pharmaceutical company research neglects rare diseases because the high cost of research and development is not recovered. A potential approach to shorten the timeline for drug discovery and reduce costs is to find new indications for existing drugs. This strategy, defined as "drug repurposing," takes advantage of the known activities of many drugs approved for human use.[24]

Herein, we used a drug-repositioning strategy combined with high-throughput screening (HTS) to identify molecules that reduce the accumulation of p62/SQSTM1 in cystinotic PTCs and restore normal autophagy. Among several positive hits, luteolin emerged as the most interesting candidate. Additional studies showed that this molecule has a good safety profile, improves the lysosome-mediated degradation of the autophagy cargoes, restores lysosomal distribution, and stimulates endocytosis in cystinotic PTCs. These results were

Significance Statement

Nephropathic cystinosis, the most severe form of the lysosomal storage disease cystinosis, presents as renal Fanconi syndrome. Defective cystine transport leads to intralysosomal accumulation and crystallization of cystine. The only treatment for cystinosis, cysteamine, does not correct the Fanconi syndrome or prevent progression to ESKD, suggesting involvement of pathways unrelated to lysosomal cystine accumulation. The authors used high-throughput screening to identify molecules that reduce accumulation of the autophagy substrate p62/SQSTM1 in cystinotic proximal tubular epithelial cells and restore normal autophagy. Studies in cells derived from patients with, or mouse models of, cystinosis and in cystinotic zebrafish indicate that luteolin corrects aspects of the cystinotic phenotype that are linked to renal Fanconi syndrome. These findings provide new perspectives for the treatment of nephropathic cystinosis and other renal lysosomal storage diseases.

further validated *in vivo* on a previously established zebrafish model of cystinosis.[25]

These insights offer new opportunities for the treatment of cystinosis and other lysosomal storage diseases.

METHODS

Cell Culture and Reagents

Conditionally immortalized proximal tubular epithelial cells (ciPTCs), from healthy donors and patients with cystinosis were obtained from Radboud University Medical Center, Nijmegen, The Netherlands, and cultured as described in Wilmer *et al.*[26] We used ciPTCs bearing the classic homozygous −57 kb deletion ($CTNS^{-/-}$ ciPTC). Human cystinotic fibroblasts were kindly provided by laboratorio di Diagnosi Pre e Postnatale delle Malattie Metaboliche, Istituto G. Gaslini, Italy. Fibroblasts were cultured as previously described.[27]

Lymphocytes obtained by venous blood from healthy donors and patients with cystinosis were collected in preservative-free anticoagulant tubes and then layered onto Histopaque-1077 solution. After centrifugation at $400 \times g$ for 30 minutes at room temperature, lymphocytes and other mononuclear cells were collected at the plasma/Histopaque-1077 interface, washed with PBS (Euroclone), and transferred into RPMI (Euroclone) supplemented with 10% FBS (Gibco), 100 U/ml penicillin, and 100 mg/ml streptomycin (Euroclone). Cells were grown in a humidified atmosphere with 5% CO_2 at 37°C. mPTCs derived from age- and sex-matched $Ctns^{-/-}$ and wild-type littermates (C57BL/6 background). Mice were maintained under temperature- and humidity-controlled conditions with 12-hour light/dark cycles with free access to appropriate standard diet in accordance with the institutional guidelines of National Institutes of Health Guide for the Care and Use of Laboratory Animals. The kidneys were harvested from wild-type and $Ctns^{-/-}$ mice (aged 16 weeks) and were taken to generate primary cultures of mPTCs, as previously described.[21] Luteolin was purchased from Shaanxi

Huike Botanical Development Co., Ltd, Xi'an, Shaanxi (China); HBSS, for starvation experiments, was purchased from Euroclone; TNFα, for apoptosis induction, was purchased from Peprotech; and all other reagents were purchased from Sigma-Aldrich (St. Louis, MO).

RNA Extraction, Quantitative Real-Time PCR, and Western Blotting
RNA extraction, quantitative real-time PCR, and Western blotting are described in Supplemental Appendix 1.

Fluorescence Assays
Fluorescence assays and microscopy analysis are described in Supplemental Appendix 1.

Screening of the Prestwick Chemical Library in ciPTCs
The Prestwick Chemical Library was purchased from Prestwick Chemical (Illkirch-Graffenstaden, France) and consisted of a collection of 1200 off-patent small molecules, 95% of which are approved for human use by the US Food and Drug Administration, European Medicines Agency, and other agencies. Twenty-four hours after seeding in 96-well plates, each molecule of the library was added to the ciPTCs at final concentration of 10 μM, using the epMotion 5075 automated pipetting system.

We included eight wells with *Ctrl* ciPTCs as a positive control and eight wells with $CTNS^{-/-}$ ciPTCs as a negative control, in columns 1 and 12 of each plate, respectively, both treated with DMSO 0.1% v/v, the vehicle in which compounds are dissolved. After 24 hours, we evaluated p62/SQSTM1 protein levels, normalized for number of cells, spectrophotometrically, by in-cell ELISA assay (in Cell-ELISA color detection kit; Thermo Fisher Scientific), according to the manufacturer's instructions. The values of p62/SQSTM1 under treatment with each drug of the library were normalized respect to the average of controls (p62/SQSTM1 level in $CTNS^{-/-}$ ciPTCs) of the same plate.

Measurement of Intracellular and Mitochondrial Reactive Oxygen Species
Cellular reactive oxygen species (ROS) generation was detected by CellROX Deep Reagent (C10422; Thermo Fisher Scientific) and CellROX Green Reagent (C10444; Thermo Fisher Scientific), and mitochondrial ROS were detected by MitoSOX Red Mitochondrial Superoxide Indicator (M36008; Thermo Fisher Scientific), according to the manufacturer's instructions. Protocol details are described in Supplemental Appendix 1.

Endocytosis Assays
HA-Meg4 binding assay and BSA uptake were performed as described in Supplemental Appendix 1.

Fish Maintenance and Breeding
Ctns$^{-/-}$ and wild-type adult zebrafish were raised at 28.5°C, on a 14/10-hour light/dark cycle under standard aquaculture conditions. After mating, every 20–30 fertilized embryos were transferred per well of a six-well plate having approximately

5 ml of clean egg water (Instant Ocean Sea Salts, 60 μg/ml) and methylene blue (0.5 ppm). Embryos were incubated at 28.5°C in the dark and the medium was refreshed daily. Drugs were dissolved in the swimming water with the required concentrations starting from 48 hours postfertilization (hpf). Every day the debris was removed, and dead embryos were sorted out and counted. Survival was monitored over the first 144 hpf. Hatching rates were calculated in surviving embryos at 48, 72, and 96 hpf, and deformity rates were evaluated at 96 hpf. All larval experiments were performed between the third and the sixth days postfertilization (dpf). Animal care and experimental procedures were conducted in accordance with the ethical committee guidelines for laboratory animal experimentation at Katholieke Universiteit Leuven and the reference European Union directive (Directive 2010/63/EU) on the protection of animals used for scientific research.

Evaluation of Apoptosis in Zebrafish Larvae
Cell death was evaluated by caspase-3 enzyme activity, as described in Supplemental Appendix 1.

Immunohistofluorimetric Staining of Larval Renal Proximal Tubules for Megalin, Early Endosomal Antigen-1 and Ras-Related Protein-11
Wild-type and *ctns*$^{-/-}$ zebrafish larvae (either nontreated or treated with 100 μM luteolin) at 5 dpf were fixed and stained for megalin, early endosomal antigen-1 (EEA1), and Ras-related protein-11 (Rab11) antibody, as described in Supplemental Appendix 1.

Statistical Analyses
To monitor the performance of the screening, we used the Z'-factor statistical parameter.[28] Z'-factor was evaluated by using the formula $Z' = 1 - 3 \times (\sigma_p + \sigma_n)/|\mu_p - \mu_n|$, where σ_p and σ_n are the SDs of the positive or negative sample, and μ_p and μ_n represent the averages. GraphPad Prism software was used for all statistical analyses. The results are expressed as means$\pm$SEM and they are representative of at least three independent experiments, unless otherwise specified in the figure legends. Differences between experimental groups were evaluated using one-way ANOVA followed by Bonferroni when appropriate. When only two groups were compared, unpaired or paired two-tailed *t* tests were used for numerical data, and Fisher exact and chi-squared tests were used for categorical data as appropriate. All differences were considered statistically significant with $P < 0.05$.

RESULTS

Cell-Based Drug Screening for Molecules that Reduce p62/SQSTM1 Levels
p62/SQSTM1 protein levels were analyzed in ciPTCs obtained from a healthy donor (*Ctrl*) and a patient with cystinosis with a homozygous −57 kB *CTNS* deletion ($CTNS^{-/-}$ ciPTC). In-cell ELISA experiments showed significantly increased levels

in cells derived from patient with cystinosis, compared with those obtained from healthy donor (Figure 1A). mRNA levels were unchanged (Supplemental Figure 1A). Increased accumulation of p62/SQSTM1 in cystinosis was further confirmed by Western blot (Figure 1B). Notably, treatment with 100 μM cysteamine for 24 hours did not significantly modify p62/SQSTM1 levels (Figure 1B) despite a significant decrease in cystine levels (Supplemental Figure 1B), indicating that the accumulation of this protein is not directly related to lysosomal cystine accumulation.

After inhibition of mRNA synthesis for 24 hours with actinomycin D, p62/SQSTM1 protein levels remained higher in $CTNS^{-/-}$ ciPTCs compared with $Ctrl$, indicating that the accumulation was not related to higher mRNA transcription (Supplemental Figure 1, C and D). Moreover, p62/SQSTM1 levels decreased significantly in $Ctrl$ after 4 hours of starvation in HBSS, whereas they remained higher in $CTNS^{-/-}$ ciPTCs (Supplemental Figure 1E), suggesting impaired autophagic flux.

This was further supported by bafilomycin and by chloroquine treatments that increased p62/SQSTM1 protein levels in $Ctrl$ but had no effect on the already elevated levels of $CTNS^{-/-}$ ciPTCs (Supplemental Figure 1, F and G). Of notice, increased levels of p62/SQSTM1 were specific to ciPTCs and were not increased in other cell types, such as lymphocytes and fibroblasts, obtained from patients with cystinosis (Supplemental Figure 1H).

Quantitative in-cell ELISA was performed to identify drug that decrease p62/SQSTM1 levels in cystinotic cells. The Z'-factor value for the in-cell ELISA assay was 0.62 ± 0.06, demonstrating the robustness of the assay. Screening was performed in triplicates on $CTNS^{-/-}$ ciPTCs, using the Prestwick Chemical Library (Figure 1C). Using a threshold for positivity of 50% reduction in p62/SQSTM1 levels above levels in $Ctrl$ cells, we identified 46 positive compounds (Supplemental Table 1). After discarding molecules with a low therapeutic range and a restricted topical use, six molecules were retained for additional studies (Figure 1, D and E). Among these, luteolin emerged as a particularly interesting candidate.

Taken together, these results showed that degradation of the autophagic substrate p62/SQSTM1 is compromised in ciPTCs. Drug screening revealed luteolin as the best candidate to rescue this phenotype.

Luteolin Has a Favorable Toxicity Profile

The effect of luteolin on p62/SQSTM1 levels was analyzed in $CTNS^{-/-}$ ciPTC using a dose-response inhibition model, which revealed a half-maximal inhibitory concentration of 127 μM (Supplemental Figure 2A).The toxicity profile was also analyzed on ciPTCs showing a half-maximal inhibitory concentration of 170 μM and 189 μM for $Ctrl$ and $CTNS^{-/-}$ ciPTC, respectively (Supplemental Figure 2B). In mPTCs, no substantial changes in cell viability after 24 hours were noticed at 20 μM, and 10%–15% cell death was observed at 50 μM (Supplemental Figure 2C). Further, luteolin toxicity profile

was tested *in vivo* using the $ctns^{-/-}$ zebrafish. Survival was analyzed for 96 hours after exposing wild-type and $ctns^{-/-}$ embryos to different concentrations of luteolin in the swimming water at 48 hpf. Luteolin had no significant effect on embryos survival at concentrations of 100 μM and 500 μM (Figure 2, A and B). Moreover, luteolin improved delayed hatching and deformity rates of mutated embryos (Figure 2, C–F).

These data showed that luteolin has a good safety profile in preclinical model of cystinosis.

Luteolin Rescues Autophagic Defects in Cystinosis

Cell immunofluorescence (Figure 3, A and B) and Western blot (Supplemental Figure 3, A and B) further confirmed the effects of luteolin on p62/SQSTM1 levels in cystinotic ciPTCs (Figure 3A) and mPTCs (Figure 3B).

To further analyze autophagy, we measured LC3-II levels in mPTCs (Figure 3C). By Western blotting, LC3-II levels in $Ctns^{-/-}$ mPTCs were significantly increased compared with wild-type animals. Luteolin significantly decreased LC3-II levels. Thereafter, we transfected $CTNS^{-/-}$ ciPTCs with LC3 cDNA expressing the tandem RFP-/GFP-fluorescent tag. In this system, green fluorescence is quenched when vesicle pH decreases, indicating fusion with the lysosomal compartment. As shown in Figure 3D, the percentage of yellow positive structures (autophagosomes) was significantly higher in cystinotic cells, whereas the percentage of RFP-only positive structures (autolysosomes) was significantly lower. This was restored by luteolin treatment (Figure 3D).

These data demonstrated that the autophagic flux is impaired in ciPTCs and mPTCs. Luteolin efficiently rescued autophagic defects in these cells.

Luteolin Protects from Apoptosis

Increased susceptibility to apoptosis is a known phenotype of cystinotic cells. We therefore investigated the possible protective role of luteolin against apoptosis in $Ctrl$ and $CTNS^{-/-}$ ciPTCs. Cells were pretreated with luteolin for 6 hours and apoptosis was subsequently induced by exposure to 30 ng/ml TNFα and 2.5 μg/ml actinomycin D for 18 hours, as previously described.[9] Levels of cleaved poly-ADP-ribose polymerase (PARP-1) (Figure 4A) and cleaved caspase-3 (Supplemental Figure 4A) were assessed by Western blotting. As shown, $CTNS^{-/-}$ ciPTCs had increased activation of both PARP-1 and caspase-3 after apoptotic stimuli, compared with $Ctrl$ ciPTCs. Luteolin pretreatment significantly protected from apoptosis in stimulated cells.

Similarly, apoptosis was tested in $ctns^{-/-}$ zebrafish by measuring caspase-3 enzyme activity in larval homogenates (Figure 4B). Increased apoptotic rate was apparent at 5 dpf. Exposure to 100 and 500 μM luteolin reduced apoptosis significantly in $ctns^{-/-}$ larvae.

These data confirmed increased susceptibility of cystinotic cells and zebrafish model to apoptosis and highlighted the ability of luteolin to rescue this phenotype.
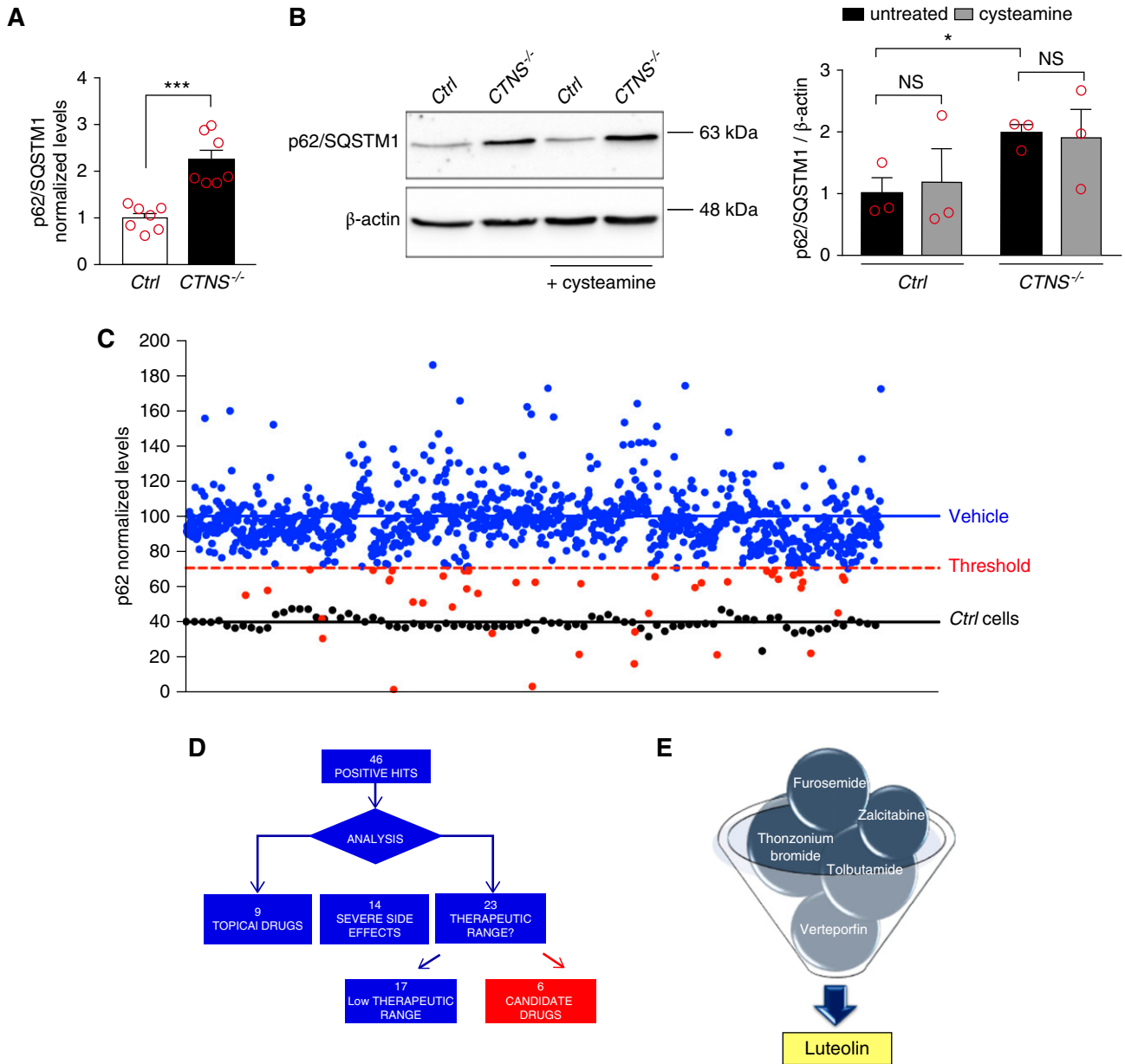
Figure 1. Cell-based phenotypic drug screening for compounds that reduce p62/SQSTM1 levels. (A) p62/SQSTM1 protein levels were analyzed in ciPTCs from a healthy donor (*Ctrl*) and a patient with cystinosis (*CTNS$^{-/-}$*) by in-cell ELISA. Levels of p62/SQSTM1 were normalized by Janus Green cell stain. Data are shown as fold change of untreated *Ctrl*. Mean values±SEM from seven independent experiments are reported. *t* test ***$P<0.001$. (B) Western blotting and densitometric analysis of p62/SQSTM1 and β-actin levels in *Ctrl* and *CTNS$^{-/-}$* ciPTC after treatment with 100 μM cysteamine for 24 hours. Histogram shows levels of p62/SQSTM1 normalized to those of β-actin and reported as relative to untreated *Ctrl* ratios. Data are shown as mean±SEM from three independent experiments. *t* test *$P<0.05$; NS not statistically significant. (C) p62/SQSTM1 levels were analyzed in *CTNS$^{-/-}$* ciPTCs after treatment with DMSO (vehicle, negative control) or 10 μM of each drug of the Prestwick Chemical Library (red and blue dots). *Ctrl* cells were used as positive control (black dots). The threshold for significance (red dashed line) was set at 50% reduction in the relative increased p62/SQSTM1 levels in *CTNS$^{-/-}$* ciPTCs (blue line) compared with *Ctrl* cells (black line). This threshold highlights 46 positive hits (red spots). Levels of p62/SQSTM1 were normalized to Janus Green cell stain signal. Data are represented as mean value of three independent experiments. (D and E) Diagram represents process of selection of six candidate drugs. The screening yielded 46 positive hits, of which nine drugs were excluded because they are registered for topical use only, 14 because of severe side effects, and 17 because of their low therapeutic range.
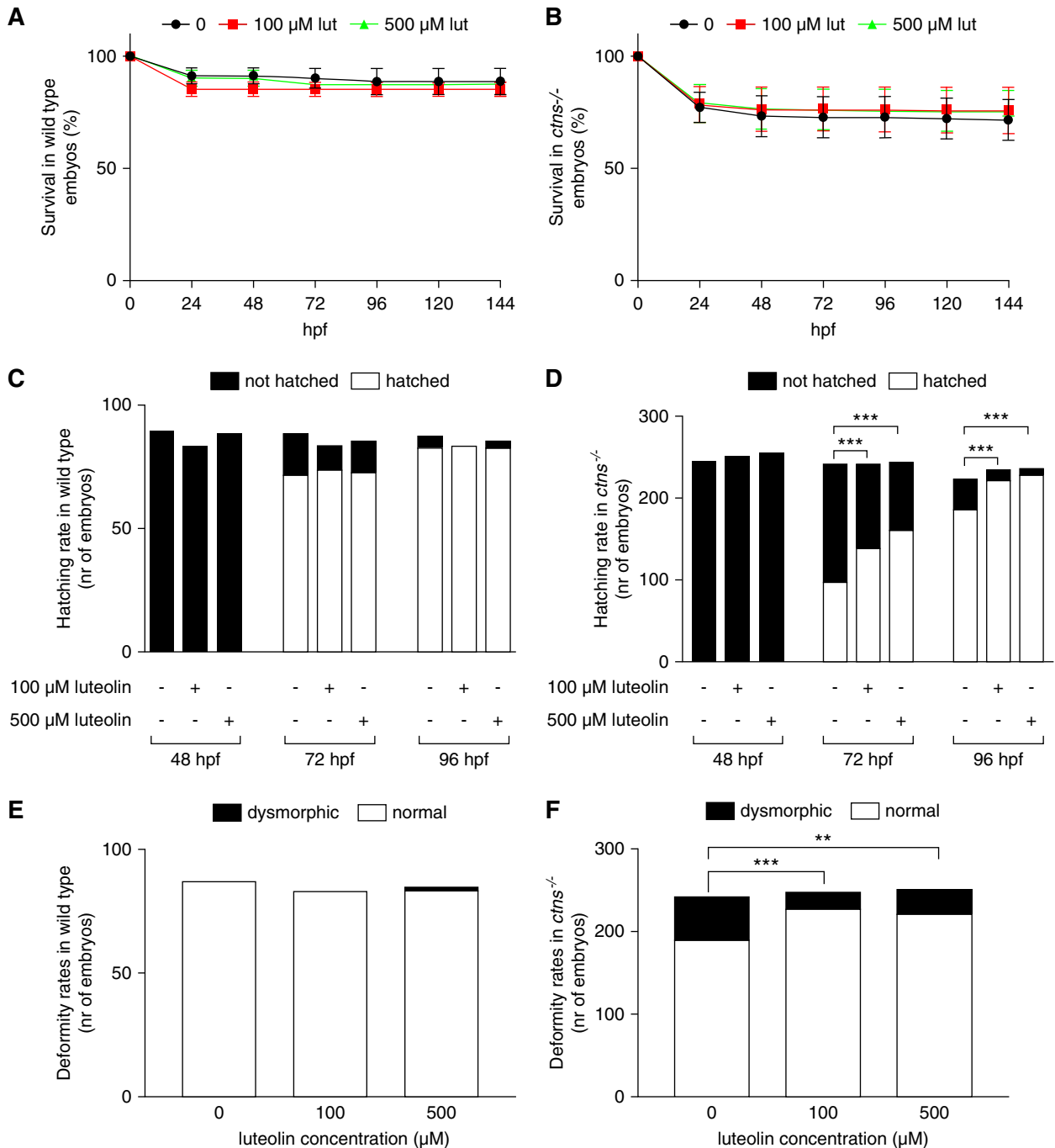
Figure 2. Luteolin has a favorable toxicity profile and improves hatching rates and deformity rates in $ctns^{-/-}$ zebrafish larvae. (A and B) Survival rates in wild-type and $ctns^{-/-}$ embryos and larvae after 0, 100, or 500 μM luteolin. Data are reported as mean±SEM (n=3 independent experiments). (C and D) Hatching rates in surviving wild-type and $ctns^{-/-}$ embryos evaluated at 48, 72, and 96 hpf with 0, 100, or 500 μM of luteolin. (E and F) Deformity rates in wild-type and $ctns^{-/-}$ larvae after 0, 100, or 500 μM luteolin. The total numbers of embryos evaluated for survival, hatching, and deformity rates were 97 embryos per group of wild-type and 350 embryos per group of $ctns^{-/-}$ zebrafish. Luteolin was administered at 48 hpf in all experiments dissolved in the swimming water with the specified concentrations. **$P<0.01$ and ***$P<0.001$ using Fisher test.

Luteolin Ameliorates Oxidative Stress in PTCs

Thereafter, we investigated the antioxidant effect of luteolin in ciPTCs using the CellROX probe. Basal cellular ROS levels were 2.2-fold higher in $CTNS^{-/-}$ ciPTC, compared with $Ctrl$ cells. As expected, ROS levels increased significantly (7.5-fold) in $CTNS^{-/-}$ ciPTCs after exposure to $tert$-butyl-hydroperoxide

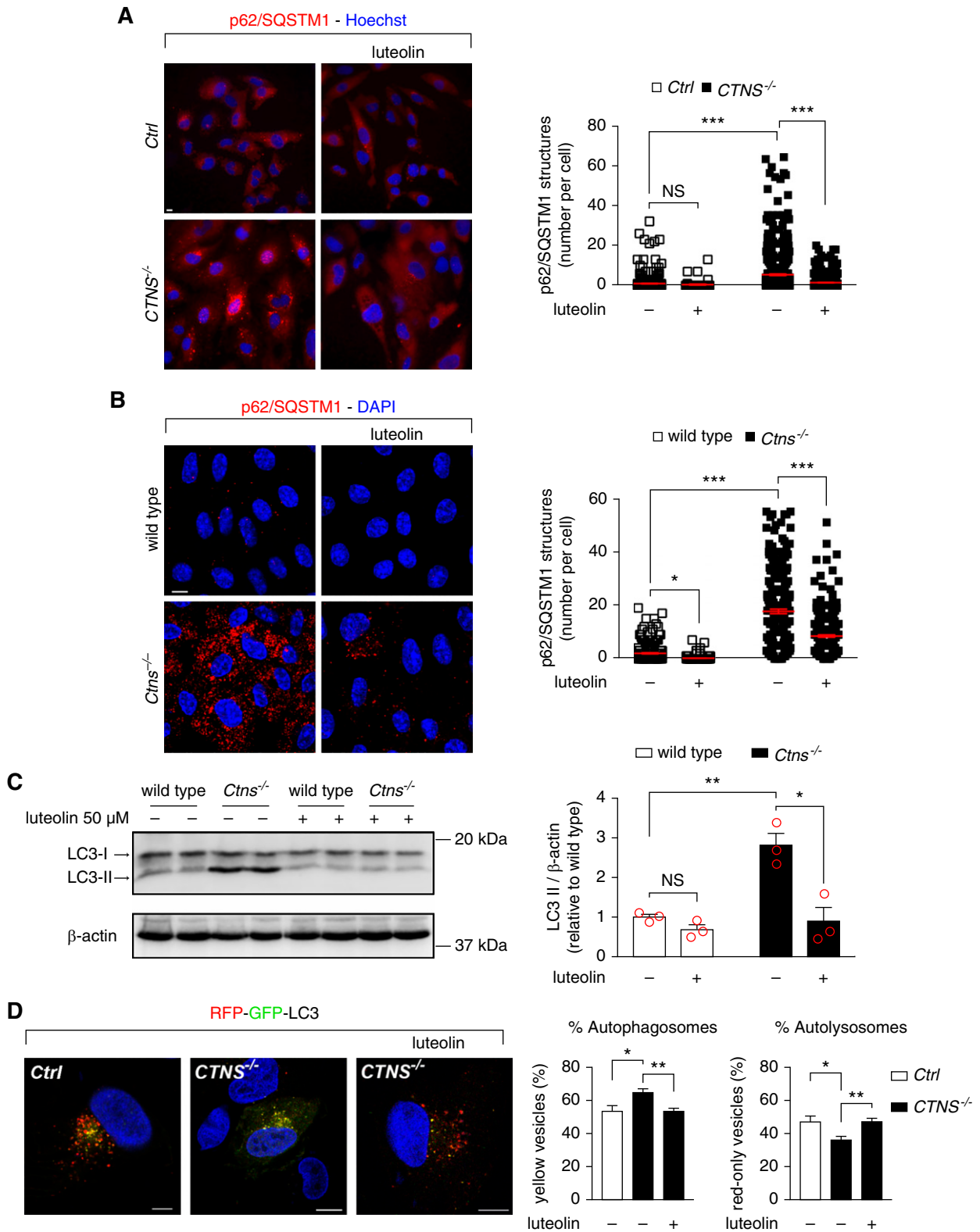**Figure 3.** Luteolin rescues autophagic defects in cystinosis. (A) Representative images of *Ctrl* and *CTNS*$^{-/-}$ ciPTCs after treatment with 50 μM luteolin for 24 hours. After fixing, cells were stained with anti-p62/SQSTM1 antibody (red) and Hoechst (nuclei, blue). Scale bar is 10 μm. Graph represents number of p62/SQSTM1-positive structures per cells (*n*>70 cells from three independent experiments, one-way ANOVA followed by Bonferroni *post hoc* test, ***P<0.001 and NS not statistically significant). (B) Representative images of wild-type and *Ctns*$^{-/-}$ mPTCs after treatment with 50 μM luteolin for 24 hours. After fixing, cells were stained with anti-p62/SQSTM1
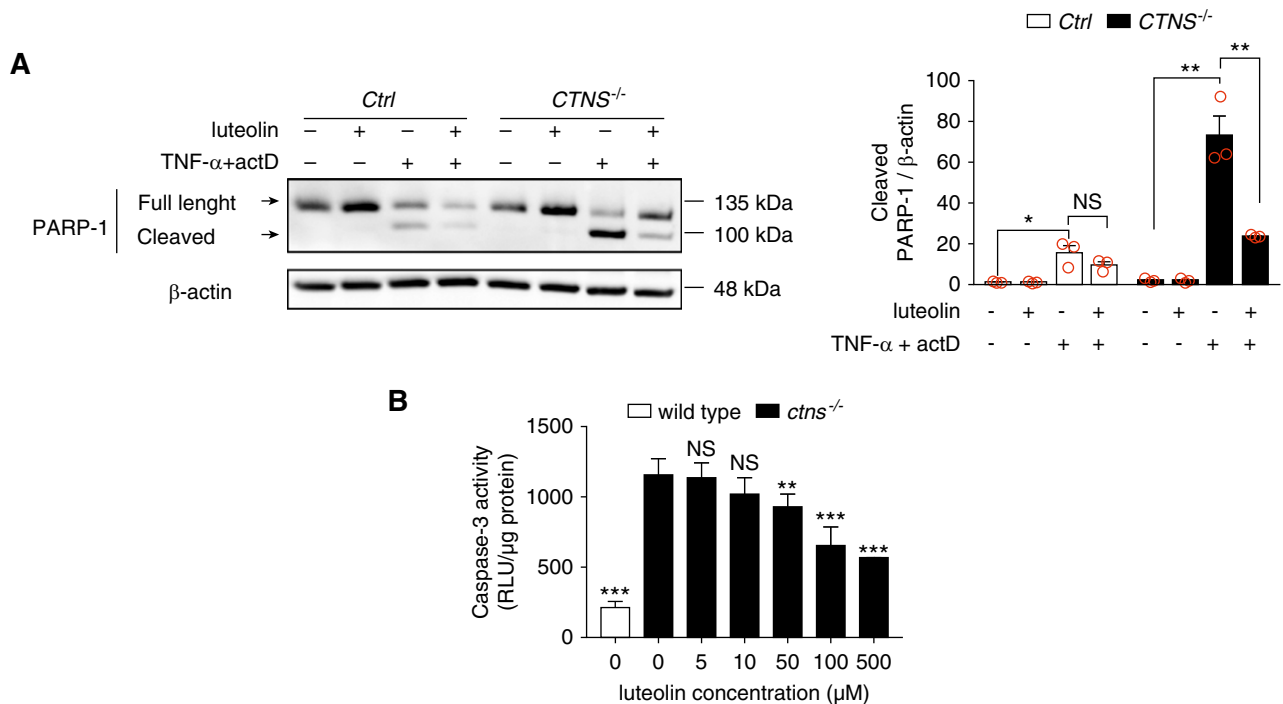
A

B

Figure 4. Luteolin reduces sensitivity to apoptosis in $CTNS^{-/-}$ ciPTCs and in $ctns^{-/-}$ zebrafish larvae. (A) Western blotting and densitometric analysis of PARP-1 and β-actin protein levels in Ctrl and $CTNS^{-/-}$ ciPTCs left untreated or pretreated with 50 μM luteolin for 6 hours. After luteolin pretreatment, where indicated apoptosis was induced by 18 hours treatment with 30 ng/ml TNFα and 2.5 μg/ml actinomycin D (actD). Histogram shows levels of cleaved PARP-1 normalized to those of β-actin and reported as relative to untreated Ctrl ratios. Data are shown as mean±SEM from three independent experiments. t test *$P<0.05$; **$P<0.01$ and NS not statistically significant. (B) Quantitation of caspase-3 enzyme activity (RLU/μg protein) in homogenates of 120 hpf wild-type and $ctns^{-/-}$ zebrafish larvae either untreated or treated with 5, 10, 50, 100, and 500 μM luteolin. Twenty larvae were homogenized in each pellet and at least three replicates were performed per condition. t test **$P<0.01$; ***$P<0.001$ and NS not statistically significant relative to untreated $ctns^{-/-}$ condition.

(Figure 5A). Pretreatment with 50 μM luteolin for 24 hours decreased cellular ROS generation by approximately 80% in both Ctrl and $CTNS^{-/-}$ ciPTCs. These findings were further confirmed under basal conditions on mPTCs by fluorescence microscopy. The CellROX signal decreased to control levels upon treatment with 50 μM luteolin for 24 hours (Figure 5B). We further monitored mitochondrial oxidative stress by MitoSOX probe. No significant difference was found in basal mitochondrial ROS levels in $CTNS^{-/-}$ ciPTC compared with Ctrl cells; nevertheless, 50 μM luteolin neutralized

mitochondrial ROS production (Supplemental Figure 4B). In $CTNS^{-/-}$ ciPTC, the exposure to tert-butyl-hydroperoxide increased mitochondrial ROS levels (3.0-fold), revealing a higher sensitivity of $CTNS^{-/-}$ ciPTCs. Pretreatment with 50 μM luteolin for 24 hours decreased mitochondrial ROS generation by approximately 80% in both Ctrl and $CTNS^{-/-}$ ciPTCs (Supplemental Figure 4B).

Taken together, these data indicated that luteolin significantly rescued the increased sensitivity to oxidative stress of both human and murine cystinotic PTCs.

antibodies (red) and DAPI (nuclei, blue). Scale bar is 10 μm. Graph represents number of p62/SQSTM1-positive structures per cell ($n>214$). One-way ANOVA followed by Bonferroni post hoc test, *$P<0.05$ and ***$P<0.001$. (C) Western blotting and densitometric analyses of LC3 and β-actin protein levels in mPTCs after treatment with 50 μM luteolin for 24 hours. Data are shown as mean±SEM ($n=3$ independent experiments), t test *$P<0.05$; **$P<0.01$ and NS not statistically significant. (D) Representative images of Ctrl and $CTNS^{-/-}$ ciPTCs transfected with RFP-GFP-LC3. After 24 hours from transient transfection, cells were left untreated or treated with 50 μM luteolin for 24 hours. Scale bar is 10 μm. GFP and RFP signals were analyzed by confocal microscopy. Percentage of autophagosomes (yellow vesicles) and percentage of autolysosomes (red-only vesicles) were calculated on the basis of the ratio between the number of yellow and red-only puncta, respectively, and the total number of autophagosomes (number of yellow and red-only puncta). Data are reported as mean±SEM ($n>70$ cells from five independent experiments). One-way ANOVA followed by Bonferroni post hoc test, **$P<0.01$ and *$P<0.05$.
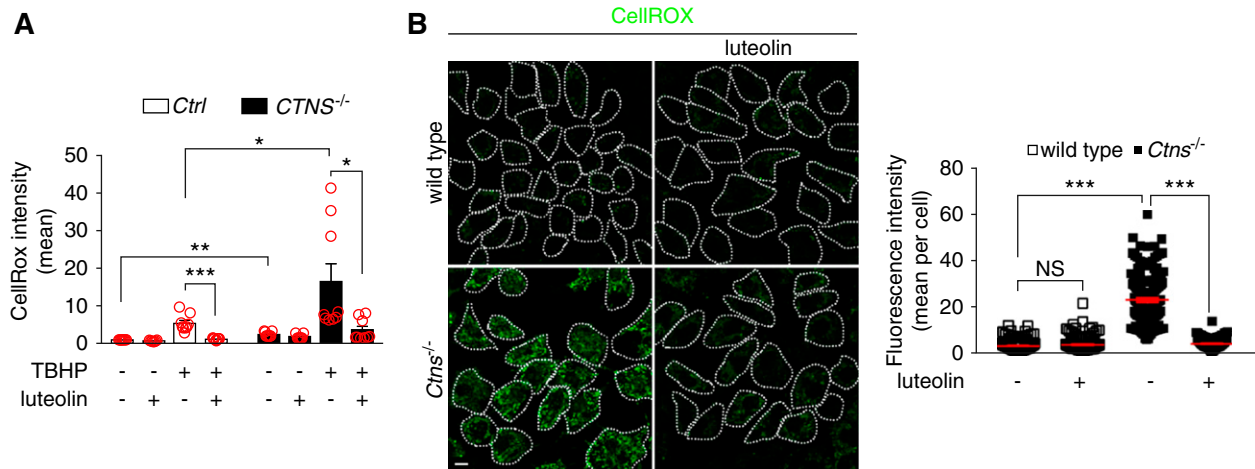
Figure 5. Luteolin treatment reduces oxidative stress in cystinotic cells. (A) *Ctrl* and *CTNS*^{−/−} ciPTCs were left untreated or pretreated with 50 μM luteolin for 24 hours. Levels of cellular ROS were then analyzed both at basal conditions and after 2 hours exposure to 100 μM *tert*-butyl- hydroperoxide (TBHP) by CellROX staining and flow cytometry. Diagram shows CellROX mean intensities normalized to those of untreated *Ctrl*. Data are presented as mean±SEM from nine independent experiments. *t* test *$P<0.05$; **$P<0.01$; and ***$P<0.001$. (B) Representative images and quantification of CellROX (green) staining in wild-type and *Ctns*^{−/−} mPTCs under basal condition or treatment with 50 μM luteolin for 24 hours. Scale bar is 10 μm. CellROX fluorescence intensities per cell are reported; means and SEM are shown in red (n>100 cells, one-way ANOVA followed by Bonferroni *post hoc* test, ***$P<0.001$ and NS not statistically significant).

Luteolin Improves Lysosome Dynamics and Processing in Cystinotic PTCs

Structures positive for lysosome-associated membrane protein 1 (LAMP1) were analyzed by fluorescent microscopy, after exposure to 50 μM luteolin for 24 hours. As shown in Figure 6A, distribution of enlarged perinuclear lysosomes in cystinotic cells were prevented by luteolin treatment, re-establishing a pattern of lysosomal distribution similar to control cells. This was observed both in human ciPTCs and in mPTCs. More specifically, after luteolin treatment the fraction of perinuclear lysosome decreased on average from 54% to 40% in *CTNS*^{−/−} ciPTCs (Figure 6A), and from 44% to 22% in mPTCs (Figure 6B). In addition, cathepsin-D expression was analyzed in mPTCs. The proteolytic generation of the 33-kDa mature cathepsin-D was lower in *Ctns*^{−/−} mPTCs compared with wild-type cells. Luteolin treatment restored the expression of mature cathepsin-D (Figure 6C).

Serial block-face scanning electron microscopy of the proximal region of the pronephros of *ctns*^{−/−} zebrafish larvae revealed an increase in the size of lysosomes compared with wild-type, as reported previously.[25] Treatment of the *ctns*^{−/−} larvae with luteolin (100 μM for 72 hours) partially rescued this phenotype, with a significant reduction in lysosome size compared with untreated larvae, although the lysosomes were still larger than those of wild-type larvae (Figure 7).

These data showed that luteolin reverts impaired lysosomal dynamics and morphology in cystinosis.

Luteolin Restored Megalin Expression and Enhanced Protein Reabsorption

We next evaluated surface expression of the endocytic receptor megalin, *in vitro* and *in vivo*. We first used the HA-Meg4 mini-receptor construct (an accepted surrogate for full-length megalin), transiently expressed in ciPTCs. Fluorescence intensity was measured after cell incubation on ice with anti-HA antibody. *CTNS*^{−/−} ciPTCs showed a significant reduction in relative HA-Meg4 surface levels compared with *Ctrl* cells (0.43±0.04 in *CTNS*^{−/−} cells compared with 1.18±0.10 in *Ctrl* cells), which was significantly improved by luteolin treatment (0.73±0.07; Figure 8A). Expression of endogenous megalin was also assessed in *Ctrl* and *CTNS*^{−/−} ciPTCs. Fluorescence intensity was measured after staining with anti-megalin antibody. As shown in Supplemental Figure 5A, *CTNS*^{−/−} ciPTCs showed significant reduction of expression of endogenous megalin compared with *Ctrl* cells, which was rescued by luteolin treatment. *In vivo* studies were carried out on 5 dpf *ctns*^{−/−} zebrafish larvae. As shown in Figure 8, B–D, megalin expression was grossly altered in mutated animals, with most of the signal located in subapical and intracellular vesicular structures. After treatment with luteolin, megalin expression was largely restored in the brush border membranes of *ctns*^{−/−} larvae tubular cells (Figure 8, B–D), whereas it was unchanged in wild-type larvae (data not shown). Further, luteolin treatment partially restored in *ctns*^{−/−} larvae defective expression of EEA1 and Rab11, which marks preferentially recycling endosomes (Supplemental Figure 5B). Receptor-mediated endocytosis of albumin was investigated in mPTCs. We found a reduction (approximately 85%) of fluorescent BSA uptake in *Ctns*^{−/−} mPTCs, compared with wild-type cells (Figure 8E). Pretreatment with 50 μM luteolin for 24 hours increased BSA uptake in both wild-type and *Ctns*^{−/−} mPTCs.

These data showed that trafficking of megalin to the plasma membrane is compromised in cystinosis. Luteolin efficiently
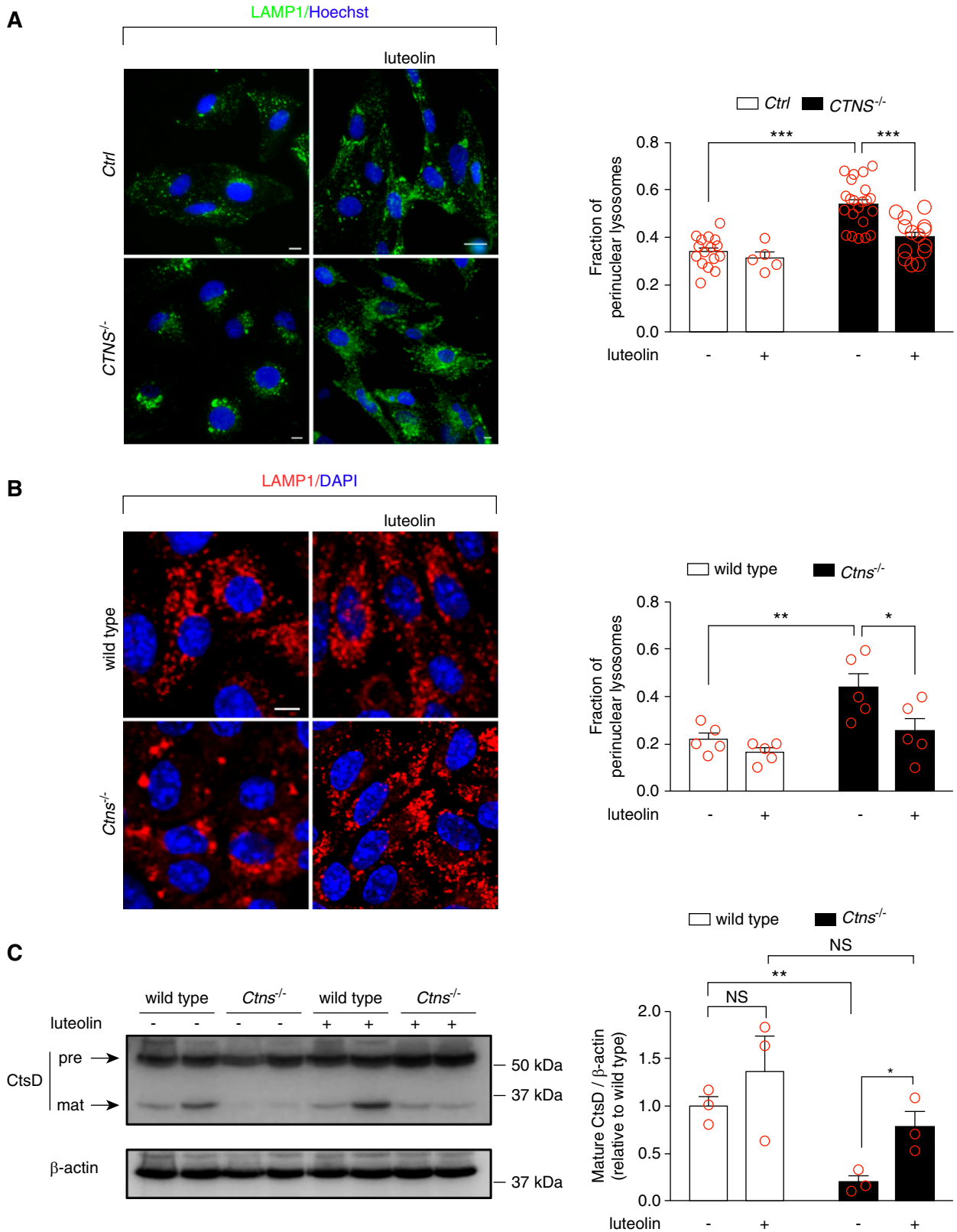
A

B

C

Figure 6. Luteolin treatment rescues morphology and degradation capacities of lysosomes in cystinotic cells. (A) Representative images of *Ctrl* and *CTNS*$^{-/-}$ ciPTCs left untreated or treated with 50 μM luteolin for 24 hours. After fixing, cells were stained with anti–lysosome-associated membrane protein 1 (LAMP1) antibody (green) and Hoechst (nuclei, blue). Scale bar is 10 μm. Fraction of perinuclear lysosomes was quantified in at least five randomly selected fields (red circles) per condition. Mean±SEM are shown by
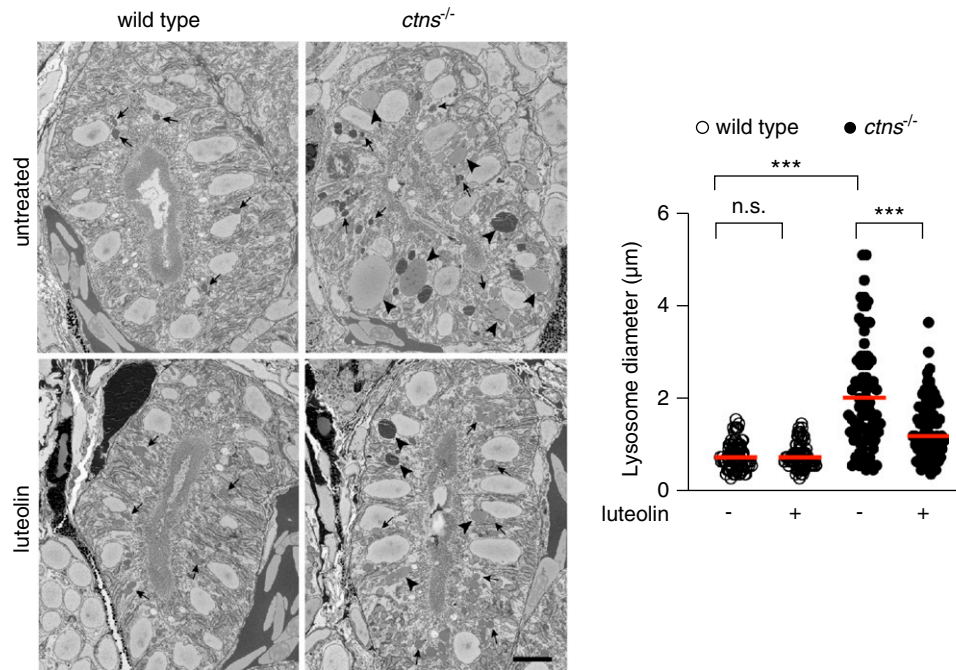
Figure 7. Luteolin restores impaired morphology of lysosomes in the pronephros of $ctns^{-/-}$ larvae. Representative block-face scanning electron microscopy images of the proximal tubule of 5 dpf wild-type and $ctns^{-/-}$ larvae after treatment without or with luteolin (100 μM for 72 hours). Arrowheads indicate lysosomes >1.5 μm diameter. Arrows indicate lysosomes <1.5 μm diameter. Scale bar is 5 μm. Diameter of lysosomes was quantified in five randomly selected fields ($n=80$ lysosomes from four tubules of two larvae for each experimental condition). Mann–Whitney U test ***$P<0.001$ and NS not statistically significant .
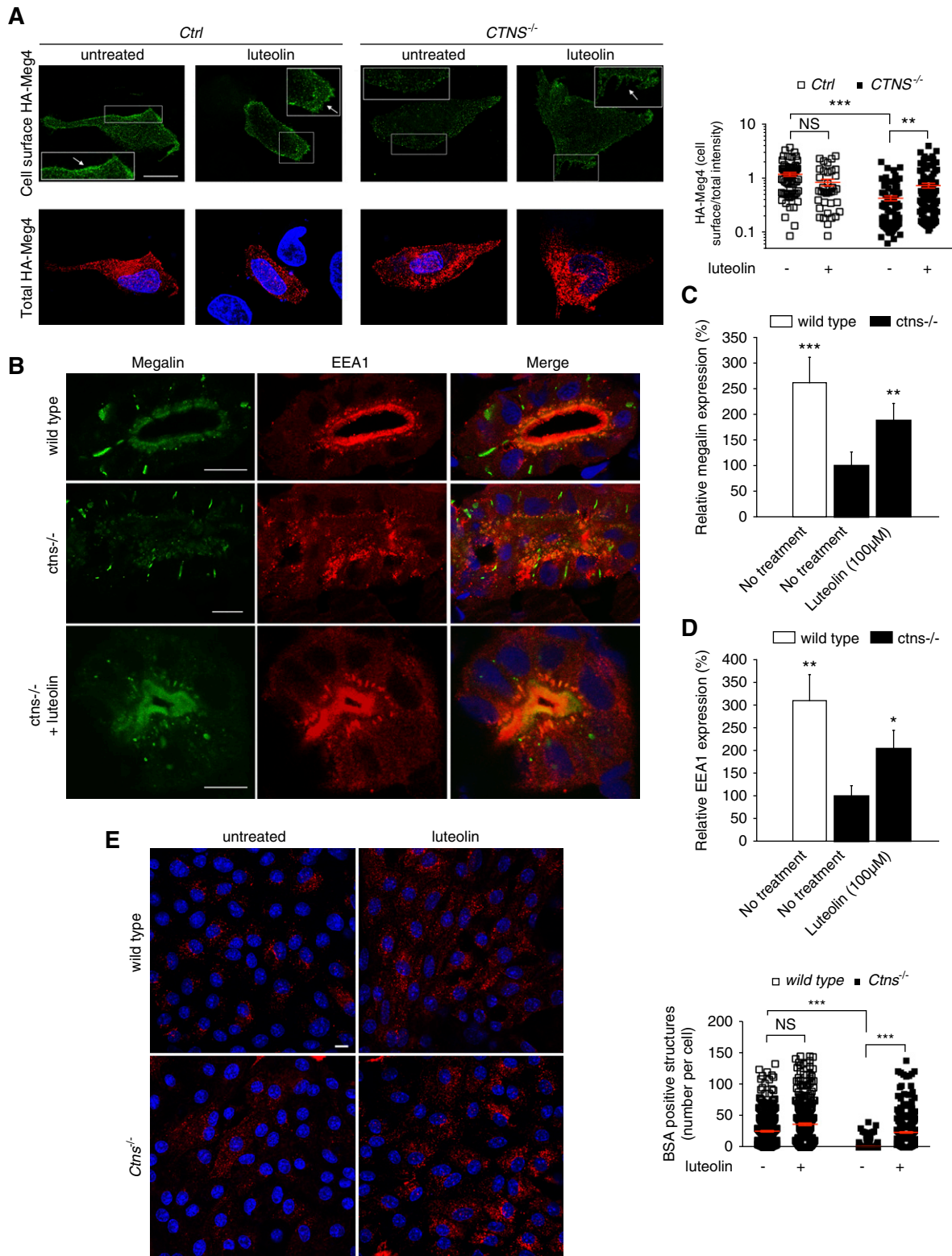
rescued localization of megalin to the plasma membrane and improved reabsorption of endocytic cargoes.

DISCUSSION

Nephropathic cystinosis is caused by lack of functional cystinosin, a cystine/H^+ symporter that allows lysosomal cystine efflux. Cysteamine is currently the only therapy available for this disease, allowing clearing of cystine from lysosomes.[29] For many years, enhanced cell oxidation has been considered a cornerstone of the disease.[14,16,17,30,31] Although results of various studies are difficult to harmonize, several experimental data show impaired response of cystinotic cells to oxidative stimuli.[17,32] A leading hypothesis for many years has been that the Cys/CySS redox state unbalance, secondary to cystine retention in lysosomes, impairs glutathione synthesis.[31–33] This hypothesis was substantiated by lower glutathione levels in

several cystinotic cell lines,[14,33–35] and by improvement of glutathione levels after treatment with N-acetyl-cysteine or with cysteamine,[31,33] which replete the cytoplasmic pool of cysteine from the external milieu or from the lysosomal compartment, respectively. More recent data, however, offer an alternative or complementary explanation, by demonstrating that lysosomal dysfunction in cystinosis compromises autophagy-mediated clearance of damaged mitochondria in PTCs, which are a potent source of ROS.[20] In this context, part of the beneficial effects of luteolin, a natural flavonoid present in various fruits and vegetables,[36] may be explained by its antioxidant properties,[37] similar to the positive effects on renal lesions reported in $Ctns^{-/-}$ mice treated with other mitochondria-targeted ROS scavengers, such as MitoTempo and mitoquinone.[20,38] The antioxidant effects of luteolin are related to its capacity to scavenge oxygen and nitrogen reactive species.[39] In ROS-insulted primary cultured neurons, for example, luteolin has been shown to decrease endogenous free radicals, to

column bars. One-way ANOVA followed by Bonferroni *post hoc* test, ***$P<0.001$. (B) Representative images of wild-type and $Ctns^{-/-}$ mPTCs under basal condition or treatment with 50 μM luteolin for 24 hours. After fixing, cells were stained with anti-LAMP1 antibody (red) and DAPI (nuclei, blue). Scale bar is 10 μm. Fraction of perinuclear lysosomes was quantified in at least five randomly selected fields (red circles) per condition. Mean±SEM are shown by column bars. One-way ANOVA followed by Bonferroni *post hoc* test, *$P<0.05$ and **$P<0.01$. (C) Western blotting and densitometric analysis of cathepsin-D (CtsD) and β-actin protein levels from wild-type and $Ctns^{-/-}$ mPTCs, left untreated or treated with 50 μM luteolin for 24 hours. Histogram shows levels of mature CtsD (33 kDa) normalized to those of β-actin and reported as relative to control wild-type ratios ($n=3$ independent experiments). t test *$P<0.05$; **$P<0.01$ and NS not statistically significant.

Figure 8. Luteolin restores endocytic defects in cystinosis. (A) *Ctrl* and *CTNS*$^{-/-}$ ciPTCs were transiently transfected with HA-Meg4. After 4–6 hours, transfection medium was replaced by full medium or 50 μM luteolin for 24 hours. The cell surface exposure of HA–Meg4 was measured through binding at 4°C (cell surface HA–Meg4) of an anti-HA mouse antibody. The total amount of HA–Meg4 expressed was measured using an anti-HA rabbit antibody (total HA–Meg4) in permeabilized HA–Meg4 cells. The arrows indicate plasma membrane localization of HA-Meg4. Scale bar is 20 μm. Histogram shows ratios of cell surface/total HA-Meg4 fluorescence

improve mitochondrial membrane potential, and to ameliorate mitochondrial viability.[40]

A second distinctive feature of cystinotic cells is their propensity to undergo apoptosis when stimulated with intrinsic or extrinsic stimuli.[8] The underlying mechanisms have been attributed to abnormal cysteinylation of protein kinase Cδ by cystine released from disrupted lysosomes.[9] Importantly, cysteamine restores normal susceptibility to apoptosis,[8] in theory by preventing lysosomal cystine accumulation and lysosomal rupture.[9] We observed that luteolin also reduces sensitivity to apoptosis in preclinical models of cystinosis. However, luteolin has no effect on cystine storage (Supplemental Figure 1B). Cysteamine has been used for the treatment of cystinosis since the 1980s and has substantially ameliorated the outcome of patients. However, despite its efficacy in lowering lysosomal cystine, cysteamine cannot cure the disease and does not prevent some aspects of the renal disease, namely the renal Fanconi syndrome.[41] These observations suggest the involvement of other cellular pathways in the pathophysiology of nephropathic cystinosis, in addition to the engulfment of the lysosomal compartment with cystine.[42,43] Therefore, research in this field is increasingly focusing on new therapies aimed at correcting cell phenotypes that are not restored by cysteamine. These include, for example, abnormal lysosomal distribution,[22] lysosome-associated membrane protein 2 mislocalization,[19] mTORC1 dysregulation,[44] impaired chaperon-mediated autophagy,[19] and abnormal level of p62/SQSTM1 in renal tubular cells. Defective lysosome-autophagy degradation pathways have been recently linked to epithelial dysfunction[20] and to renal Fanconi syndrome, often the first clinical manifestation of the disease.

This work shows that luteolin ameliorates several of the abovementioned features. This molecule (3′,4′,5,7-tetrahydroxyflavone) was identified by drug repositioning, an approach that is particularly valuable for rare diseases because it shortens the duration and cost of drug development.[24] To this end, we selected the Prestwick Chemical Library, which contains 1200 molecules, most of which have been licensed for human use, to perform an HTS on the basis of a semiautomated in-cell ELISA assay. Our phenotypic target was p62/SQSTM1 in PTCs, which was used as a marker of altered autophagy. This choice was on the basis of the recent demonstration that autophagy is heavily impaired in cystinotic cells,[18–20] a feature that is unresponsive to cysteamine as shown in our experiments. In addition, our results show that luteolin

restores the distribution of lysosomes in cystinotic PTCs, improves megalin expression, and enhances endo-lysosomal trafficking processes. In immune cells, luteolin has also been shown to inhibit cytokine expression, NF-κB activation, and TLR4 signaling at micromolar concentrations.[45] The exact mechanisms by which luteolin exerts its polyhedral effects are not completely understood.

Impaired autophagy is a key feature in lysosomal storage diseases, including cystinosis, and is secondary to altered delivery of cargoes to the engulfed lysosomal compartment.[20,46] Sansanwal and Sarwal[18] had already observed increased levels of p62/SQSTM1 in cystinotic renal PTCs, and in renal biopsy specimens obtained from patients with cystinosis. Importantly, this finding is not ubiquitous and is restricted to some cells, including renal PTCs. For example, Napolitano et al.[19] observed normal macro-autophagy and normal autophagic flux in cystinotic fibroblasts. Similarly, we also observed comparable p62/SQSTM1 levels in lymphocytes and fibroblasts obtained from patients with cystinosis and from controls. These data suggest that lack of cystinosin determines tissue- and cell-specific effects.

Our data show that luteolin significantly improves the autophagic flux in cystinotic PTCs, resulting in decreased p62/SQSTM1 accumulation. Luteolin has also been shown to increase the number of autolysosomes and to promote autophagy in human cutaneous squamous carcinoma cells.[47] These effects were blocked by chloroquine, an inhibitor of the last steps of the autophagic process.[47] Similarly, luteolin was also found to protect mice from traumatic brain injury, an effect that was attributed to its anti-inflammatory properties,[36] but was also associated with an increased number of LC3-positive cells and decreased levels of p62/SQSTM1.[48]

In addition, the distribution of lysosomes normalized after treatment with luteolin in our cell models, most likely because of improved functionality, as indicated by mature cathepsin-D levels. Recently, Janssens et al.[49] showed that inhibition of megalin-mediated endocytosis efficiently prevents accumulation of cystine and delays progression of kidney disease in Ctns^{−/−} mice. In these experiments, ablation of megalin was used as a strategy to block uptake of proteins, whose degradation further increases cystine contents in Ctns^{−/−} mice. In cystinosis, defective expression of megalin has been well documented, including in reports by the same authors.[23,42] Lack of megalin expression reflects impaired intracellular trafficking and membrane protein recycling, similarly to what is observed

---

intensity (n>65 cells for each experimental condition). t test **P<0.01; ***P<0.001 and NS not statistically significant . (B) Representative confocal images of the protein expression of the multiligand receptor megalin (green) and EEA1 (red) in wild-type larvae, untreated ctns^{−/−} larvae, and luteolin-treated (100 μM) ctns^{−/−} larvae. Scale bar is 5 μm in all images. Quantitation of periluminal fluorescence intensity at the level of the proximal tubules of (C) megalin (n=8 larvae/group) and (D) EEA1 (n=4 larvae/group). Relative fluorescence intensities in quantitation graphs were referred to the untreated ctns^{−/−} group, which was considered as 100%. t test *P<0.05; **P<0.01; and ***P<0.001. (E) Representative images of BSA uptake (red) in wild-type and Ctns^{−/−} mPTCs under basal condition or treatment with 50 μM luteolin for 24 hours. Scale bar is 10 μm. Number of BSA-positive structures per cell was quantified; mean and SEM are shown in red (n>300 cells, one-way ANOVA followed by Bonferroni post hoc test, ***P<0.001 and NS not statistically significant).

in other proximal tubular defects characterized by low-molecular-weight proteinuria, such as Lowe syndrome and Dent disease.[50] In addition, lack of megalin expression may also indicate cell dedifferentiation, as shown in mPTCs by Raggi *et al.*[21] Therefore, and irrespective of the underlying mechanism, restored expression of megalin after *in vitro* and *in vivo* treatments in our experimental settings indicates that luteolin may be efficient in treating the renal Fanconi syndrome of cystinosis and is not at odds with the report by Janssens *et al.*[49]

In conclusion, luteolin was selected from the positive hits of an HTS aimed at improving autophagy because of its additional effects on oxidation, apoptosis, and inflammation, all of which are altered in cystinosis.[8–11,14–17,32,45,51–53] Moreover, luteolin belongs to the flavonoid family, similar to genistein, which we recently showed to ameliorate lysosomal cystine content and lysosomal compartment distribution in cystinosis, likely through stimulation of the TFEB pathway.[27] Flavonoids have been proposed for the treatment of other lysosomal storage diseases[54,55] and luteolin has been shown to have a very good safety profile in humans.[56,57] Taken together, our results indicate that luteolin may be valuable for the treatment of cystinosis, in particular to ameliorate aspects of the disease that are not improved by cysteamine and establish a proof of principle to begin preclinical studies *in vivo*.

DISCLOSURES

All authors have nothing to disclose.

SUPPLEMENTAL MATERIAL

This article contains the following supplemental material online at http://jasn.asnjournals.org/lookup/suppl/doi:10.1681/ASN.2019090956/-/DCSupplemental.

Supplemental Figure 1. Levels of p62/SQSTM1 are specifically increased in human cystinotic PTCs.

Supplemental Figure 2. Toxicity profile of luteolin.

Supplemental Figure 3. Treatment with luteolin reduces p62/SQSTM1 levels in both human and mouse PTCs.

Supplemental Figure 4. Luteolin treatment reduces sensitivity to apoptosis and mitochondrial ROS in cystinotic cells.

Supplemental Figure 5. Luteolin treatment restores endocytic defects in $CTNS^{-/-}$ ciPTCs $ctns^{-/-}$ zebrafish larvae.

Supplemental Table 1. List of the 46 best hits yielded by HTS.

Supplemental Appendix 1. Supplemental materials and methods, and references.

REFERENCES

1. Emma F, Nesterova G, Langman C, Labbé A, Cherqui S, Goodyer P, et al.: Nephropathic cystinosis: An international consensus document. *Nephrol Dial Transplant* 29[Suppl 4]: iv87-iv94, 2014

2. Kalatzis V, Cherqui S, Antignac C, Gasnier B: Cystinosin, the protein defective in cystinosis, is a H(+)-driven lysosomal cystine transporter. *EMBO J* 20: 5940–5949, 2001

3. Gahl WA, Thoene JG, Schneider JA: Cystinosis. *N Engl J Med* 347: 111–121, 2002

4. Brodin-Sartorius A, Tête MJ, Niaudet P, Antignac C, Guest G, Ottolenghi C, et al.: Cysteamine therapy delays the progression of nephropathic cystinosis in late adolescents and adults. *Kidney Int* 81: 179–189, 2012

5. Elmonem MA, Veys KR, Soliman NA, van Dyck M, van den Heuvel LP, Levtchenko E: Cystinosis: A review. *Orphanet J Rare Dis* 11: 47, 2016

6. Dohil R, Fidler M, Gangoiti JA, Kaskel F, Schneider JA, Barshop BA: Twice-daily cysteamine bitartrate therapy for children with cystinosis. *J Pediatr* 156: 71–75–3, 2010

7. Rocca CJ, Cherqui S: Potential use of stem cells as a therapy for cystinosis. *Pediatr Nephrol* 34: 965–973, 2019

8. Park M, Helip-Wooley A, Thoene J: Lysosomal cystine storage augments apoptosis in cultured human fibroblasts and renal tubular epithelial cells. *J Am Soc Nephrol* 13: 2878–2887, 2002

9. Park MA, Pejovic V, Kerisit KG, Junius S, Thoene JG: Increased apoptosis in cystinotic fibroblasts and renal proximal tubule epithelial cells results from cysteinylation of protein kinase Cdelta. *J Am Soc Nephrol* 17: 3167–3175, 2006

10. Thoene JG: Lysosomal cystine augments apoptosis and causes the phenotype in cystinosis. *Beijing Da Xue Xue Bao* 37: 8–9, 2005

11. Taranta A, Bellomo F, Petrini S, Polishchuk E, De Leo E, Rega LR, et al.: Cystinosin-LKG rescues cystine accumulation and decreases apoptosis rate in cystinotic proximal tubular epithelial cells. *Pediatr Res* 81: 113–119, 2017

12. Bellomo F, Signorile A, Tamma G, Ranieri M, Emma F, De Rasmo D: Impact of atypical mitochondrial cyclic-AMP level in nephropathic cystinosis. *Cell Mol Life Sci* 75: 3411–3422, 2018

13. De Rasmo D, Signorile A, De Leo E, Polishchuk EV, Ferretta A, Raso R, et al.: Mitochondrial dynamics of proximal tubular epithelial cells in nephropathic cystinosis. *Int J Mol Sci* 21: E192, 2019

14. Wilmer MJ, de Graaf-Hess A, Blom HJ, Dijkman HB, Monnens LA, van den Heuvel LP, et al.: Elevated oxidized glutathione in cystinotic proximal tubular epithelial cells. *Biochem Biophys Res Commun* 337: 610–614, 2005

15. Sansanwal P, Li L, Hsieh SC, Sarwal MM: Insights into novel cellular injury mechanisms by gene expression profiling in nephropathic cystinosis. *J Inherit Metab Dis* 33: 775–786, 2010

16. Vaisbich MH, Pache de Faria Guimaraes L, Shimizu MH, Seguro AC: Oxidative stress in cystinosis patients. *Nephron Extra* 1: 73–77, 2011

17. Sumayao R, McEvoy B, Newsholme P, McMorrow T: Lysosomal cystine accumulation promotes mitochondrial depolarization and induction of redox-sensitive genes in human kidney proximal tubular cells. *J Physiol* 594: 3353–3370, 2016

18. Sansanwal P, Sarwal MM: p62/SQSTM1 prominently accumulates in renal proximal tubules in nephropathic cystinosis. *Pediatr Nephrol* 27: 2137–2144, 2012

19. Napolitano G, Johnson JL, He J, Rocca CJ, Monfregola J, Pestonjamasp K, et al.: Impairment of chaperone-mediated autophagy leads to selective lysosomal degradation defects in the lysosomal storage disease cystinosis. *EMBO Mol Med* 7: 158–174, 2015

20. Festa BP, Chen Z, Berquez M, Debaix H, Tokonami N, Prange JA, et al.: Impaired autophagy bridges lysosomal storage disease and epithelial dysfunction in the kidney. *Nat Commun* 9: 161, 2018

21. Raggi C, Luciani A, Nevo N, Antignac C, Terryn S, Devuyst O: Dedifferentiation and aberrations of the endolysosomal compartment characterize the early stage of nephropathic cystinosis. *Hum Mol Genet* 23: 2266–2278, 2014

22. Ivanova EA, De Leo MG, Van Den Heuvel L, Pastore A, Dijkman H, De Matteis MA, et al.: Endo-lysosomal dysfunction in human proximal tubular epithelial cells deficient for lysosomal cystine transporter cystinosin. *PLoS One* 10: e0120998, 2015

23. Gaide Chevronnay HP, Janssens V, Van Der Smissen P, N'Kuli F, Nevo N, Guiot Y, et al.: Time course of pathogenic and adaptation mechanisms in cystinotic mouse kidneys. *J Am Soc Nephrol* 25: 1256–1269, 2014

24. Bellomo F, Medina DL, De Leo E, Panarella A, Emma F: High-content drug screening for rare diseases. *J Inherit Metab Dis* 40: 601–607, 2017

25. Elmonem MA, Khalil R, Khodaparast L, Khodaparast L, Arcolino FO, Morgan J, et al.: Cystinosis (ctns) zebrafish mutant shows pronephric glomerular and tubular dysfunction. *Sci Rep* 7: 42583, 2017

26. Wilmer MJ, Saleem MA, Masereeuw R, Ni L, van der Velden TJ, Russel FG, et al.: Novel conditionally immortalized human proximal tubule cell line expressing functional influx and efflux transporters. *Cell Tissue Res* 339: 449–457, 2010

27. Rega LR, Polishchuk E, Montefusco S, Napolitano G, Tozzi G, Zhang J, et al.: Activation of the transcription factor EB rescues lysosomal abnormalities in cystinotic kidney cells. *Kidney Int* 89: 862–873, 2016

28. Zhang JH, Chung TD, Oldenburg KR: A simple statistical parameter for use in evaluation and validation of high throughput screening assays. *J Biomol Screen* 4: 67–73, 1999

29. Gahl WA, Reed GF, Thoene JG, Schulman JD, Rizzo WB, Jonas AJ, et al.: Cysteamine therapy for children with nephropathic cystinosis. *N Engl J Med* 316: 971–977, 1987

30. Sumayao R Jr., Newsholme P, McMorrow T: The role of cystinosin in the intermediary thiol metabolism and redox homeostasis in kidney proximal tubular cells. *Antioxidants* 7: E179, 2018

31. Bellomo F, Corallini S, Pastore A, Palma A, Laurenzi C, Emma F, et al.: Modulation of CTNS gene expression by intracellular thiols. *Free Radic Biol Med* 48: 865–872, 2010

32. Mannucci L, Pastore A, Rizzo C, Piemonte F, Rizzoni G, Emma F: Impaired activity of the gamma-glutamyl cycle in nephropathic cystinosis fibroblasts. *Pediatr Res* 59: 332–335, 2006

33. Chol M, Nevo N, Cherqui S, Antignac C, Rustin P: Glutathione precursors replenish decreased glutathione pool in cystinotic cell lines. *Biochem Biophys Res Commun* 324: 231–235, 2004

34. Levtchenko E, de Graaf-Hess A, Wilmer M, van den Heuvel L, Monnens L, Blom H: Altered status of glutathione and its metabolites in cystinotic cells. *Nephrol Dial Transplant* 20: 1828–1832, 2005

35. Laube GF, Shah V, Stewart VC, Hargreaves IP, Haq MR, Heales SJ, et al.: Glutathione depletion and increased apoptosis rate in human cystinotic proximal tubular cells. *Pediatr Nephrol* 21: 503–509, 2006

36. López-Lázaro M: Distribution and biological activities of the flavonoid luteolin. *Mini Rev Med Chem* 9: 31–59, 2009

37. Heim KE, Tagliaferro AR, Bobilya DJ: Flavonoid antioxidants: Chemistry, metabolism and structure-activity relationships. *J Nutr Biochem* 13: 572–584, 2002

38. Galarreta CI, Forbes MS, Thornhill BA, Antignac C, Gubler MC, Nevo N, et al.: The swan-neck lesion: Proximal tubular adaptation to oxidative stress in nephropathic cystinosis. *Am J Physiol Renal Physiol* 308: F1155–F1166, 2015

39. Ashaari Z, Hadjzadeh MA, Hassanzadeh G, Alizamir T, Yousefi B, Keshavarzi Z, et al.: The flavone luteolin improves central nervous system disorders by different mechanisms: A review. *J Mol Neurosci* 65: 491–506, 2018

40. Zhao G, Yao-Yue C, Qin GW, Guo LH: Luteolin from Purple Perilla mitigates ROS insult particularly in primary neurons. *Neurobiol Aging* 33: 176–186, 2012

41. Cherqui S: Cysteamine therapy: A treatment for cystinosis, not a cure. *Kidney Int* 81: 127–129, 2012

42. Cherqui S, Courtoy PJ: The renal Fanconi syndrome in cystinosis: Pathogenic insights and therapeutic perspectives. *Nat Rev Nephrol* 13: 115–131, 2017

43. Wilmer MJ, Emma F, Levtchenko EN: The pathogenesis of cystinosis: Mechanisms beyond cystine accumulation. *Am J Physiol Renal Physiol* 299: F905–F916, 2010

44. Andrzejewska Z, Nevo N, Thomas L, Chhuon C, Bailleux A, Chauvet V, et al.: Cystinosin is a component of the vacuolar H+-ATPase-ragulator-rag complex controlling mammalian target of rapamycin complex 1 signaling. *J Am Soc Nephrol* 27: 1678–1688, 2016

45. Nabavi SF, Braidy N, Gortzi O, Sobarzo-Sanchez E, Daglia M, Skalicka-Woźniak K, et al.: Luteolin as an anti-inflammatory and neuroprotective agent: A brief review. *Brain Res Bull* 119: 1–11, 2015

46. Settembre C, Fraldi A, Jahreiss L, Spampanato C, Venturi C, Medina D, et al.: A block of autophagy in lysosomal storage disorders. *Hum Mol Genet* 17: 119–129, 2008

47. Verschooten L, Barrette K, Van Kelst S, Rubio Romero N, Proby C, De Vos R, et al.: Autophagy inhibitor chloroquine enhanced the cell death inducing effect of the flavonoid luteolin in metastatic squamous cell carcinoma cells. *PLoS One* 7: e48264, 2012

48. Xu J, Wang H, Lu X, Ding K, Zhang L, He J, et al.: Posttraumatic administration of luteolin protects mice from traumatic brain injury: Implication of autophagy and inflammation. *Brain Res* 1582: 237–246, 2014

49. Janssens V, Gaide Chevronnay HP, Marie S, Vincent MF, Van Der Smissen P, Nevo N, et al.: Protection of cystinotic mice by kidney-specific megalin ablation supports an endocytosis-based mechanism for nephropathic cystinosis progression. *J Am Soc Nephrol* 30: 2177–2190, 2019

50. De Matteis MA, Staiano L, Emma F, Devuyst O: The 5-phosphatase OCRL in Lowe syndrome and Dent disease 2. *Nat Rev Nephrol* 13: 455–470, 2017

51. Lin P, Tian XH, Yi YS, Jiang WS, Zhou YJ, Cheng WJ: Luteolin-induced protection of H_2O_2-induced apoptosis in PC12 cells and the associated pathway. *Mol Med Rep* 12: 7699–7704, 2015

52. Kim S, Chin YW, Cho J: Protection of cultured cortical neurons by luteolin against oxidative damage through inhibition of apoptosis and induction of heme oxygenase-1. *Biol Pharm Bull* 40: 256–265, 2017

53. Prencipe G, Caiello I, Cherqui S, Whisenant T, Petrini S, Emma F, et al.: Inflammasome activation by cystine crystals: Implications for the pathogenesis of cystinosis. *J Am Soc Nephrol* 25: 1163–1169, 2014

54. Moskot M, Montefusco S, Jakóbkiewicz-Banecka J, Mozolewski P, Węgrzyn A, Di Bernardo D, et al.: The phytoestrogen genistein modulates lysosomal metabolism and transcription factor EB (TFEB) activation. *J Biol Chem* 289: 17054–17069, 2014

55. Piotrowska E, Jakóbkiewicz-Banecka J, Barańska S, Tylki-Szymańska A, Czartoryska B, Wegrzyn A, et al.: Genistein-mediated inhibition of glycosaminoglycan synthesis as a basis for gene expression-targeted isoflavone therapy for mucopolysaccharidoses. *Eur J Hum Genet* 14: 846–852, 2006

56. Taliou A, Zintzaras E, Lykouras L, Francis K: An open-label pilot study of a formulation containing the anti-inflammatory flavonoid luteolin and its effects on behavior in children with autism spectrum disorders. *Clin Ther* 35: 592–602, 2013

57. Marchezan J, Winkler Dos Santos EGA, Deckmann I, Riesgo RDS: Immunological dysfunction in autism spectrum disorder: A potential target for therapy. *Neuroimmunomodulation* 25: 300–319, 2018

AFFILIATIONS

[1]Renal Diseases Research Unit, Bambino Gesù Children's Hospital, Istituto di Ricovero e Cura a Carattere Scientifico, Rome, Italy

[2]Department of Clinical and Chemical Pathology, Faculty of Medicine, Cairo University, Cairo, Egypt

[3]Department of Pediatric Nephrology and Development and Regeneration, University Hospitals Leuven, Leuven, Belgium

[4]Institute of Physiology, University of Zurich, Zurich, Switzerland

[5]Wellcome Trust Centre for Cell-Matrix Research, Faculty of Biology, Medicine and Health Sciences, University of Manchester, Manchester, UK

[6]Division of Pharmacology, Utrecht Institute for Pharmaceutical Sciences, Utrecht University, Utrecht, The Netherlands

[7]Confocal Microscopy Core Facility, Research Laboratories, Bambino Gesù Children's Hospital, Istituto di Ricovero e Cura a Carattere Scientifico, Rome, Italy

[8]Department of Pediatric Medicine, Laboratory of Metabolic Biochemistry Unit, Bambino Gesù Children's Hospital, Istituto di Ricovero e Cura a Carattere Scientifico, Rome, Italy

[9]Division of Molecular and Cellular Function, School of Biological Sciences, Faculty of Biology, Medicine and Health Sciences, University of Manchester, Manchester, UK

[10]Division of Nephrology, Department of Pediatric Subspecialties, Bambino Gesù Children's Hospital, Istituto di Ricovero e Cura a Carattere Scientifico, Rome, Italy

SUPPLEMENTARY MATERIALS

Supplementary figure 1

A

B

C

D

E

F

G

H

lymphocytes

fibroblasts

Supplementary figure 2

Supplementary figure 3

A

Ctrl   Ctns⁻/⁻

luteolin   -   +   -   +

p62/SQSTM1   —— 63 kDa

β-actin   —— 48 kDa

□ Ctrl   ■ CTNS⁻/⁻

p62/SQSTM1 / β-actin

**
*
**

luteolin   -   +   -   +

B

wild type   Ctns⁻/⁻   wild type   Ctns⁻/⁻

luteolin   -   -   -   -   +   +   +   +

p62/SQSTM1   —— 75 kDa

β-actin   —— 37 kDa

□ wild type   ■ Ctns⁻/⁻

p62/SQSTM1 / β-actin
(relative to wild type)

**
*
NS

luteolin   -   +   -   +

Supplementary figure 4

A

B

Supplementary figure 5

A

B

Supplementary figure legends

Supplementary figure 1: Levels of p62/SQSTM1 are specifically increased in human cystinotic PTC. (**A**) p62/SQSTM1 mRNA levels were analyzed by real-time qPCR in ciPTCs from healthy donor (*Ctrl*) and cystinotic patient (*CTNS$^{-/-}$*). Differences in p62/SQSTM1 mRNA levels between *Ctrl* and *CTNS$^{-/-}$* ciPTCs are not statistically significant (NS). Data are shown as mean ± SEM from 4 independent experiments. (**B**) Levels of cystine, normalized to mg of total proteins and reported as relative to untre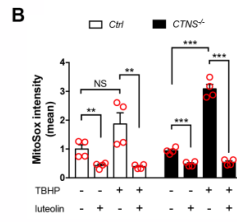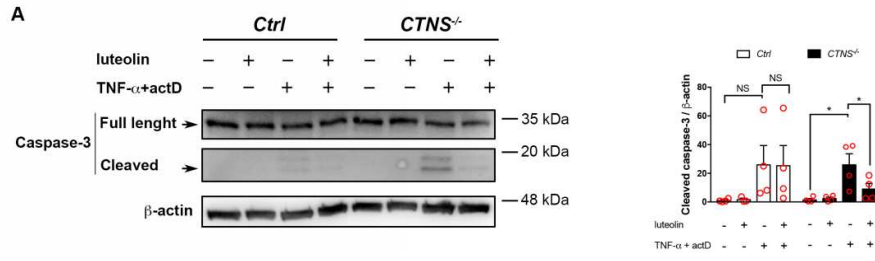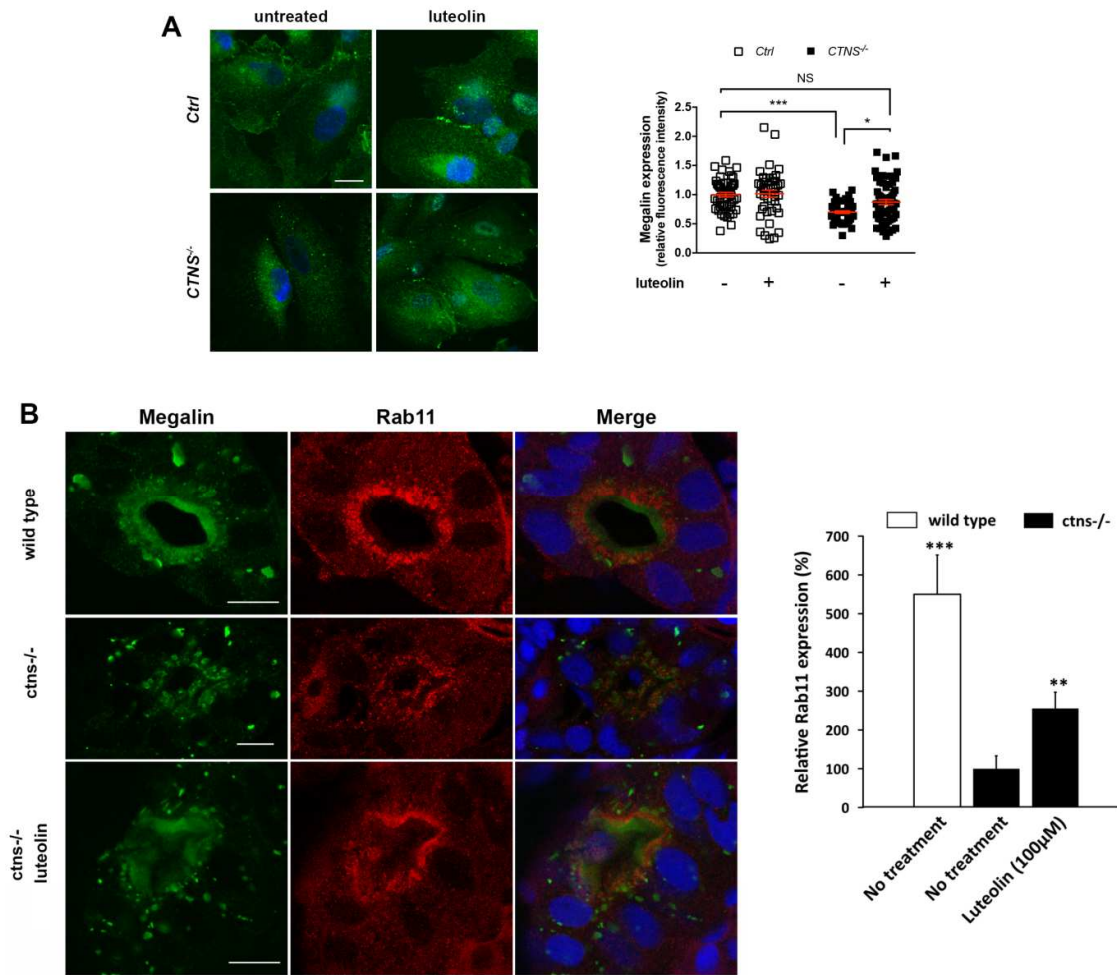ated *Ctrl*, were measured in *Ctrl* and cystinotic *CTNS$^{-/-}$* ciPTCs after treatment without or with 100μM cysteamine or 50μM luteolin for 24h. Data are shown as mean ± SEM from 6 independent experiments. Student's t test *p<0.05; **p<0.01 and NS not statistically significant. (C) p62/SQSTM1 levels were analyzed by in-Cell ELISA in *Ctrl* and *CTNS$^{-/-}$* ciPTCs after treatment with 2.5μg/ml actinomycin D for 24h. p62/SQSTM1 levels were normalized by janus green cell stain. Data are presented as mean ± SEM from 3 independent experiments, Student's t test *p<0.05; **p<0.01 and NS not statistically significant.

Western blotting and densitometric analysis of p62/SQSTM1 and β-actin protein levels in *Ctrl* and *CTNS$^{-/-}$* ciPTCs after treatment with (**D**) 2.5μg/ml actinomycin D (actD) for 24h, (**E**) Hank's salt (HBSS) for 4h, (**F**) 250nM bafilomycin A1 for 4h. Histograms show levels of p62/SQSTM1 normalized to those of β-actin and reported as relative to untreated *Ctrl* ratios. Data are shown as mean ± SEM from at least 4 independent experiments. Student's t test *p<0.05; **p<0.01 and NS not statistically significant. (**G**) p62/SQSTM1 levels were analyzed by in-Cell ELISA in *Ctrl* and *CTNS$^{-/-}$* ciPTCs after treatment with 100μM chloroquine for 24h. p62/SQSTM1 levels were normalized by janus green cell stain. Data are presented as mean ± SEM from 4 independent experiments, Student's t test *p<0.05 and NS not statistically significant. (**H**) Densitometric analysis of p62/SQSTM1 and β-actin protein levels in lymphocytes from 4 healthy donors (*Ctrl*) and 8 cystinotic patients (*CTNS$^{-/-}$*). Histogram shows levels of p62/SQSTM1 normalized to those of β-actin. Data are presented as mean ± SEM. Analysis of p62/SQSTM1 levels by in-Cell ELISA in

7

fibroblasts from two healthy donors (*Ctrl* #1 and *Ctrl* #2) and two cystinotic patients (*CTNS*^{-/-} *#1*

and *CTNS*^{-/-} *#2*). Levels of p62/SQSTM1 were normalized by janus green cell staining and shown

as mean ± SEM from 3 independent experiments, Student's t test NS not statistically significant.

Supplementary table.1 List of the 46 best hits yielded by HTS

Alexidine dihydrochloride	Lanatoside C
Alfacalcidol	Lofexidine
Atorvastatin	Luteolin
Azacytidine-5	Mebendazole
Benzathine benzylpenicillin	Merbromin
Bethanechol chloride	Methyl benzethonium chloride
Camptothecine (S, +)	Misoprostol
Chlorhexidine	Mitoxantrone dihydrochloride
Chrysene-1,4-quinone	Mometasone furoate
Cromolyn disodium salt	Pentamidine isethionate
Cycloheximide	Prazosin hydrochloride
Daunorubicin hydrochloride	Prednicarbate
Digitoxigenin	Probucol
Doxorubicin hydrochloride	Prochlorperazine dimaleate
Doxycycline hydrochloride	Proscillaridin A
Flubendazol	Serotonin hydrochloride
Fluticasone propionate	Spironolactone
Furosemide	Thonzonium bromide
Gemcitabine	Tolbutamide
Haloprogin	Topotecan
Hexetidine	Tridihexethyl chloride
Hycanthone	Verteporfin
Kanamycin A sulfate	Zalcitabine

Supplementary figure 2: Toxicity profile of luteolin. (A) p62/SQSTM1 levels were analyzed by

in-Cell ELISA in *CTNS*^{-/-} ciPTCs after treatment with increasing doses of luteolin (0; 5; 10; 20; 40;

50; 80 and 100μM) for 24h. p62/SQSTM1 levels were normalized by janus green cell stain. Data

are presented as mean ± SEM from 3 independent experiments. Half maximal inhibitory

concentration (IC$_{50}$) obtained is 127μM. (**B**) Cell viability was measured by Presto blue staining in

Ctrl (black line) and *CTNS*^{-/-} (red line) ciPTCs after 24h treatment with increasing doses of luteolin

(4.5μM; 9μM; 18μM; 37μM; 75μM; 150μM; 300μM; 600μM; 1200μM). Values were normalized to those of untreated *Ctrl* or *CTNS⁻/⁻* ciPTCs. Normalized values are reported as mean ± SEM from 3 independent experiments. Half maximal inhibitory concentration (IC_{50}) obtained is 170μM and 189μM for *Ctrl* and *CTNS⁻/⁻* ciPTC, respectively. (**C**) Cell viability as measured by MTT assay in wild type and *Ctns⁻/⁻* mPTCs after treatment with 0, 10, 20 and 50μM luteolin for 24h. Values were normalized to those of untreated wild type and *Ctns⁻/⁻* PTC. Data are reported as mean ± SEM from 3 independent experiments. Student's t test *p<0.05 and **p<0.01.

Supplementary figure 3: Treatment with luteolin reduces p62/SQSTM1 levels in both human and mouse PTCs. (**A**) Western blotting and densitometric analysis of p62/SQSTM1 and β-actin protein levels in *Ctrl* and *CTNS⁻/⁻* ciPTCs after treatment with 50μM luteolin for 24h. Histogram shows levels of p62/SQSTM1 normalized to those of β-actin and reported as relative to *Ctrl* ratios. Data are shown as mean ± SEM (n=7 independent experiments), Student's t test *p<0.05 and **p<0.01. (**B**) Western blotting and densitometric analysis of p62/SQSTM1 and β-actin protein levels in wild type and *Ctns⁻/⁻* mPTCs after treatment with 50μM luteolin for 24h. Histogram shows levels of p62/SQSTM1 normalized to those of β-actin and reported as relative to wild type ratios. Data are shown as mean ± SEM (n=3 independent experiments), Student's t test *p<0.05 and **p<0.01 and NS not statistically significant.

Supplementary figure 4: Luteolin treatment reduces sensitivity to apoptosis and mitochondrial ROS in cystinotic cells. (**A**) Western blotting and densitometric analysis of caspase-3 and β-actin protein levels in *Ctrl* and *CTNS⁻/⁻* ciPTCs left untreated or pre-treated with 50μM luteolin for 6h. After luteolin pre-treatment, where indicated apoptosis was induced by 18h treatment with 30ng/ml TNF-α and 2.5μg/ml actinomycin D (actD). Histogram shows levels of cleaved caspase-3 normalized to those of β-actin and reported as relative to untreated *Ctrl* ratios. Data are shown as mean ± SEM from 4 independent experiments. Student's t test *p<0.05;

p<0.01 and NS not statistically significant. (B**) *Ctrl* and *CTNS*$^{-/-}$ ciPTCs were left untreated or pre-treated with 50μM luteolin for 24h. Levels of mitochondrial ROS were then analyzed both at basal conditions and after 2h exposure to 100μM tert-butyl- hydroperoxide (TBHP) by MitoSOX probe and flow cytometry. Diagram shows MitoSOX mean intensities normalized to those of untreated *Ctrl*. Data are presented as mean ± SEM from 4 independent experiments. Student's t test *p<0.05; **p<0.01 and NS not statistically significant.

Supplementary figure 5: Luteolin treatment restores endocytic defects in *CTNS*$^{-/-}$ ciPTCs and *ctns*$^{-/-}$ zebrafish larvae. (**A**) Representative images of *Ctrl* and *CTNS*$^{-/-}$ ciPTCs after treatment with 50μM luteolin for 24h. After fixing, cells were stained with anti-megalin antibody (green) and Hoechst (nuclei, blue). Scale bar is 20μm. Relative fluorescence intensities per cell are shown in the graph (n>40 cells from 3 independent experiments for each condition). Mean ± SEM are shown in red. One-way ANOVA followed by Bonferroni's post hoc test, *p<0.05; ***p<0.001. (**B**) Representative confocal images of the protein expression of the multiligand receptor megalin (green) and Ras-related protein-11 (Rab11, red) in wild type larvae, untreated *ctns*$^{-/-}$ larvae and luteolin (100μM) treated larvae. Scale bar is 5μm in all images. Quantitation of peri-luminal fluorescent intensity at the level of the proximal tubules of Rab11 (n=4 larvae/group). Relative fluorescence intensities in quantitation graphs were referred to the untreated *ctns*$^{-/-}$ group, which was considered as 100%. Student's t test **p<0.01 and ***p<0.001.

Supplemental Appendix 1

SUPPLEMENTARY MATERIAL AND METHODS, AND REFERENCES

Antibody

The following antibodies were used in this study for human cells experiments: rabbit anti-Caspase-3 (9662 Cell Signaling), mouse anti- p62/SQSTM1 (sc-28359 Santa Cruz Biotechnology), mouse anti-LAMP1 (sc-20011 Santa Cruz Biotechnology), rabbit anti- LC3 (NB100-2220 Novus), rabbit anti-megalin antibody (ab76969 Abcam), rabbit anti Poly [ADP-ribose] polymerase 1 (PARP-1) (9542 Cell Signaling), mouse anti-HA Tag (32-6700 Thermofisher), rabbit anti HA-Tag (3724 Cell signaling), mouse anti-β-actin (AM4302 Ambion).

The following antibodies were used for mPTC experiments: rabbit anti-LC3 (PM036, MBL), rabbit anti-p62/SQSM1 (PM045, MBL); goat anti-Cathepsin-D (sc-6486, Santa Cruz Biotechnology); mouse anti-β-actin (A2228, Sigma-Aldrich). The following antibodies were used for zebrafish experiments: rabbit anti-megalin (kindly provided by Michele Marino, University of Pisa, Italy) and goat anti-EEA1 (Santa Cruz Biotechnology, Dallas, TX, USA), mouse anti-Rab11 (BD Biosciences Pharmingen, San Jose, CA, USA).

RNA extraction and quantitative real-time PCR

Total RNA was extracted by TRIzol reagent (Ambion, Life Technologies, Foster, CA) and cDNA was synthesized using the Euro-Script RT-PCR kit (EuroClone, Milano, Italy) according to the manufacturer's instructions. Quantitative PCR assays were performed by FAST STAR SYBR Green Master (Roche) using the following primers for SQSTM1 gene: Forward: 5'CAGATGGAGTCGGATAAC-3' and Reverse: 5'-CTGGAGTTCACCTGTAGA-3'. Gene expression data were determined using the $2^{-\Delta\Delta Ct}$ method and normalized using human glyceraldehyde-3-phosphate dehydrogenase, (GAPDH) with following primers Forward: 5'-AGGTCGGAGTCAACGGATTT -3'; Reverse: 5'-GCCCAATACGACCAAATCCG -3'.

Western blotting

Proteins were extracted lysing the cells in ripa buffer, containing proteases and phosphatases inhibitor (Thermo scientific), sonicated for 2min and centrifuged for 10min at 13,000rpm at 4°C.

Protein concentrations were measured using the Bio-Rad Protein Assay (Bio-Rad Laboratories, Inc., Hercules, CA). Proteins were separated under reducing condition by electrophoresis on 4-15% gradient gels (Bio-Rad) and immunoblotted onto polyvinylidene difluoride membranes. The membranes were blocked with 5% non-fat milk (cell signaling) diluted in Tris-buffered saline, 0.1% Tween 20 and incubated overnight with primary antibodies. Following the incubation with horseradish peroxidase secondary antibody conjugate IgG (Santa Cruz Biotechnology, Inc., Santa Cruz, CA). Immunoblots were developed with LiteAblot EXTEND (EuroClone, Milan, Italy) and acquired with the ChemiDoc XRS System (Bio-Rad). Quantification of relative density of each band normalized to β-actin, with Image Lab software (Bio-Rad).

Immunofluorescence

For immunofluorescence assay, ciPTCs were grown on glass coverslips, fixed with 4% paraformaldehyde (PFA) and permeabilized for 30min with phosphate-buffered saline containing 0.05% saponin, 0.5% bovine serum albumin, 50mM NH4Cl and incubated for 2h with appropriate primary antibody. After repeated washing with PBS, the slides were incubated for 30 min with the suitable fluorophore-conjugated Alexa secondary antibodies (Molecular probe). Nuclei were stained by Hoechst 33342, trihydrochloride, trihydrate (Invitrogen). At least 5 images per condition were acquired on a Nikon Eclipse E600 microscope (Nikon Instruments, Melville, NY) equipped with epifluorescence optics. p62/SQSTM1 number per cells was analyzed by a dedicated pipeline created with the open-source cell image analysis software CellProfiler™. LAMP1 distribution was evaluated with ImageJ software (National Institute of Health, Bethesda, MD), calculating total number of LAMP1 structure per cells and number of LAMP1 structures in defined peri-nuclear region (area within 10 μm of the nucleus).

For immunofluorescence, the mPTCs were fixed for 10min with 4% paraformaldehyde in PBS, quenched with 50mM NH4Cl and permeabilized for 30min in blocking buffer solution containing 0.1% Triton X-100 and 0.5% BSA dissolved in PBS. Subsequently, mPTCs were incubated

overnight with the appropriate primary antibodies at 4°C. After repeated washing with PBS, the slides were incubated for 30min with the suitable fluorophore-conjugated Alexa secondary antibodies (Invitrogen), mounted with the Prolong Gold Anti-fade reagent, and analyzed by using a Leica SP8 confocal laser scanning microscope (Center for Microscopy and Image Analysis, University of Zurich). The quantitative cell image analyses were performed using the open-source cell image analysis software CellProfiler[TM]. The pipeline "Cell/particle counting and scoring the percentage of stained objects" was used to score the numbers of LAMP1 and p62/SQSTM1 positive vesicles. The specific module "Measure-Object-Intensity-Distribution" was used to score the number of LAMP1 positive structures contained into perinuclear region (area within 10μm of the nucleus).

Determination of mature autophagosome

Tandem fluorescently tagged RFP-GFP-LC3 (ptfLC3), in which LC3 is expressed as a fusion protein with both GFP and RFP in tandem[1] was a gift from Tamotsu Yoshimori (Addgene plasmid Cat # 21074). ciPTCs were transfected with ptfLC3 vector by Lipofectamine LTX and Plus Reagent (Invitrogen) according to the manufacturer's instructions. After 16h of transient transfection, ciPTC were treated with 50µM luteolin (Xi'an, Shaanxi, China) for indicated time. After fixing, the glass coverslips were acquired by confocal microscopy using Olympus Fluoview FV1000 and FV10-ASW4.1 software (Olympus Corporation, Tokyo, Japan). Images were processed with ImageJ software (National Institute of Health, Bethesda, MD). The percentage of autophagosomes (yellow vesicles) and the percentage of autolysosomes (red-only vesicles) were calculated based on the ratio between the number of yellow and red-only puncta, respectively, and the total number of autophagosomes (number of yellow + red-only puncta).

Endocytosis assays

HA-tagged Meg4 plasmid and pcDNA3-RAP were kindly provided by Marzolo MP (Universidad Católica de Chile, Santiago, Chile). ciPTCs were transiently transfected with HA-Meg4 and pcDNA3-RAP a megalin chaperone, to facilitate the transport of newly synthesized Meg4 to the cell surface[2]. After 4-6h, transfection medium was replaced by full medium or 50µM luteolin for 24h. Cells were serum starved for 2h at 37°C in serum-free DMEM F12, then washed twice in cold PBS with 1% BSA chilled to 4°C and incubated with the anti-HA rabbit antibody for 1h on ice. The unbound antibody was rinsed off with cold DMEM. After binding assays, the cells were fixed, permeabilized, and stained with an anti-HA mouse, followed by goat anti-mouse Alexa-Fluor-555 (to detect total levels of expressed HA-Meg4) and anti-rabbit Alexa-Fluor-488 antibody (to detect bound anti-HA antibody).

The endocytic capacity of mPTCs was examined by measuring albumin uptake. mPTCs, previously starved for 1h in HBSS, were incubated with 100µg/mL Alexa555-BSA (A34786, Thermo Fisher Scientific) diluted in cell culture medium without FBS supplementation, for 15min at 37°C. After washing three times in PBS and once in acid solution (150mM NaCl, 10mM acetic acid, pH 3.5), the mPTCs were fixed in 4% PFA for 10min (room temperature). After three times washing in PBS, mPTCs were counterstained with 1µM DAPI for 5min, mounted with the Prolong Gold Anti-fade reagent and processed for confocal microscopy.

Measurement of intracellular reactive oxygen species (ROS)

Generation of intracellular or mitochondrial ROS in ciPTC, were detected by CellRox ® Deep Reagent (Thermo Fisher Scientific) or by MitoSOX ™ Red Mitochondrial Superoxide Indicator (M36008, ThermoFisher Scientific), respectively. ciPTCs were untreated or pre-treated for 22h with 50µM luteolin, before addition of 100µM tert-Butyl hydroperoxide (Thermo Fisher Scientific). Two h later, the cells were pulsed with 2.5µM CellRox ® Deep Reagent or 5µM MitoSOX ™ and the plate were incubated for 30min at 37°C in the dark. Once washed twice with phosphate-buffered

saline (PBS) and detached by trypsin–EDTA (Euroclone), the cells were immediately analyzed by flow cytometry BD FACSCanto II System; (BD Biosciences, San Jose, CA, USA). Ten thousand data points were collected for each sample and analyzed with FACSDiva software (BD Biosciences, San Jose, CA, USA). To detect ROS in mPTC, the cells were pulsed with 5μM CellROX® Green Reagent (C10444, Thermo Fisher Scientific) for 10min in live cell imaging at 37°C. After washing three times, the cells were subsequently analyzed by confocal microscopy. The fluorescence intensity was quantified by using ImageJ Shortcut software.

Viability assays

Cell viability assays in ciPTCs and in mPTCs treated with different concentration of luteolin, were performed by Presto Blue® reagent (Thermo Fisher Scientific) and Thiazolylbluetetrazolium bromide (MTT) reagent respectively, in according with manufacturer's instruction.

LC-MS determination of cystine

For cystine measurements, the cells were sonicated in the presence of 10mmol/l N-ethylmaleimide. The protein fraction was precipitated by the addition of 10% 5-sulfosalicylic acid and measured using the Bio-Rad Protein Assay. The supernatant (50μl) was was spiked with 50μL of the internal standard solution (Cystine d6) and vortexed for 5sec; then the mixture was extracted with 200µl of acetonitrile, vortexed at least 30sec, and then centrifuged at 13,000rpm for 9min. Liquid chromatography and mass spectrometry analysis was performed by a UHPLC Agilent 1290 Infinity II 6470 (Agilent Technologies) equipped with an ESI-JET-STREAM source operating in the positive ion (ESI+) mode. The software used for controlling this equipment and analyzing data was MassHunter Workstation (Agilent Technologies). The separation column was InfinityLab Poroshell 120 HILIC 1.9μm 100x2.1mm (Agilent Technologies). Method validation was performed based on the US Food and Drug Administration (FDA) guideline for industry bioanalytical method validation (FDA 2013) and European Medicines Agency (EMA) guideline (EMA 2011). The validation of the

assay was performed including selectivity, specificity, linearity and limit of quantification, accuracy and precision, matrix effects and recovery, and stability.

Evaluation of apoptosis in zebrafish larvae

Caspase-3 enzyme activity. At 5dpf, wild type and *ctns*$^{-/-}$ larvae (untreated or treated with 5, 10, 50, 100 or 500µM of luteolin) were homogenized in RIPA buffer. Twenty larvae were homogenized per 300µl of the buffer and at least three replicates were performed for each condition. After centrifugation (10min, 4°C, 12,000g), supernatants were preserved at −20°C until time of analysis. Caspase-3 enzyme activity were assayed in 1/100 dilution of the supernatant of each homogenate using a commercial luciferase-based assay (Caspase-Glo® 3/7, Promega, Madison, WI, USA) according to manufacturer's protocol. Luminescence was measured using the FlexStation-3 microplate reader (Molecular Devices LLC, San Jose, CA, USA). Enzyme activities were expressed in luminescence units (RLU)/µg protein for each sample, and averages were compared with the untreated *ctns*$^{-/-}$ condition.

Immunohistofluorometric staining of larval renal proximal tubules for megalin, early endosomal antigen-1 (EEA1) and Ras-related protein-11 (Rab11)

Five dpf wild type and *ctns*$^{-/-}$ (either non-treated or treated with 100µM luteolin) zebrafish larvae were fixed using 4% PFA overnight at 4°C (n= 8 larvae per group). In short, larvae were washed 3 x 5min in PBS then incubated in 30% sucrose at 4°C for a maximum of 3 days. Larvae were then embedded in 15% cold-water fish gelatin/15% sucrose, oriented in parallel in cryosection molds and frozen rapidly over a metal surface on dried ice. Frozen larvae were cut within 24h using the Leica CM3050 S cryotome (Leica Microsystems, Wetzlar, Germany). Sections were stained for a combination of rabbit anti-megalin antibody and goat anti- EEA1 antibody or a combination of rabbit anti-megalin antibody and mouse anti-Rab11 antibody. Slides were kept overnight at 4°C then washed and incubated for 3h at room temperature with the secondary antibody. Secondary

antibodies were Alexa-488 anti-rabbit (1:200), Alexa 594 anti-sheep (1:600) and Alexa 594 anti-mouse (1:600) for megalin, EEA1 and Rab11, respectively (Thermo Fisher Scientific, Waltham, MA, USA). Images were taken using confocal microscopy (Leica SP5, Leica Microsystems, Wetzlar, Germany).

Block face scanning electron microscopy

Samples were prepared and imaged with the help of the EM Facility at the Faculty of Life Sciences, University of Manchester, UK as previously described.[3] Briefly, five days post fertilization larvae were fixed in 2.5% glutaraldehyde, 4% formaldehyde in 0.1 HEPES, pH 7.2, before high density staining for serial block face imaging based on Williams et al.[4] This involved en-bloc staining with reduced osmium, thiocarbohydrazide, osmium, uranyl acetate and lead aspartate, followed by dehydration in staged ethanol (30-100%) and embedding in Epon 812 Hard formulation. Following embedding the samples were mounted on 3view pins and trimmed to locate the pronephros. A Gatan 3view mounted within a FEI Quanta 250FEG was used to collect images every 5 µm. Images were of each pronephros were collected with a field of view selected to encompass the extent of the pronephros (6000x6000 to 8000x8000 pixels) with 12nm pixel resolution. Inverted back-scattered electron images were collected at high vacuum with an accelerating voltage of 3.8kV, and a 2µs dwell time. Images were batch converted to tifs in Digital Micrograph and analyzed using ImageJ.

References

1. Kimura S, Noda T, Yoshimori T: Dissection of the autophagosome maturation process by a novel reporter protein, tandem fluorescent-tagged LC3. *Autophagy* 3: 452-460, 2007

2. Marzolo MP, Yuseff MI, Retamal C, Donoso M, Ezquer F, Farfan P, Li Y, Bu G: Differential distribution of low-density lipoprotein-receptor-related protein (LRP) and megalin in polarized epithelial cells is determined by their cytoplasmic domains. *Traffic* 4: 273-288, 2003

3. De Leo MG, Staiano L, Vicinanza M, Luciani A, Carissimo A, Mutarelli M, Di Campli A, Polishchuk E, Di Tullio G, Morra V, Levtchenko E, Oltrabella F, Starborg T, Santoro M, Di Bernardo D, Devuyst O, Lowe M, Medina DL, Ballabio A, De Matteis MA. Autophagosome-lysosome fusion triggers a lysosomal response mediated by TLR9 and controlled by OCRL. *Nat Cell Biol.* 18(8):839-850, 2016.

4. Williams ME, Wilke SA, Daggett A, Davis E, Otto S, Ravi D, Ripley B, Bushong EA, Ellisman MH, Klein G, Ghosh A. Cadherin-9 regulates synapse-specific differentiation in the developing hippocampus. *Neuron* 71: 640–655, 2011